Background

Protein ubiquitination plays a crucial role in numerous cellular processes such as cell growth, regulation of diverse signal transduction and disease [1-3]. The covalent attachment of ubiquitin to protein substrates requires a stepwise cascade of enzymatic reactions. First, ubiquitin is activated by E1 (ubiquitin-activating enzyme, UBA) in an ATP-dependent manner by forming a high-energy thioester-bond between the carboxyl-terminal glycine residue of ubiquitin and a cysteine residue of E1. The activated ubiquitin is then transferred to the core-cysteine residue of E2 (ubiquitin-conjugating enzyme, UBC). Together with an E3 ligase enzyme, ubiquitin is attached via its carboxyl-terminus to an e-amino group of a lysine residue in the target protein. Since E3 binds to both E2 and the target protein, and acts as scaffold between E2 and the substrate protein, the E3 ligase is the major determinant for selecting target proteins for ubiquitination. There is large number of genes encoding E3 ligases in all eukaryotes, and the diversity of E3s is thought to contribute to the substrate specificity of numerous target proteins. E3 ligases are structurally divided into three groups: HECT, RING and U-box [4]. The HECT-type E3 ligase is distinct from the other two ligases in that it forms a thioester-bond with ubiquitin prior to the transfer of ubiquitin to target proteins. The RING-type E3 ligase contains a unique domain similar to the zinc finger motif that mediates protein-protein interactions [5] and is further divided into two classes: one that can function alone and another that forms a complex with other E3 components [4].

Recent studies have shown that attachment of polyubiquitin chains on target proteins linked via lysine-48 of ubiquitin typically leads to degradation by the 26S proteasome [6], whereas linkage via lysine-63 mediates different pathways such as internalization of membrane proteins, activation of signal transduction and DNA damage repair [7]. The formation of lysyl-63-linked polyubiquitin chains is generated by specific combinations of E2s and E2 variants, which are similar to E2s except that they lack core cysteine residues required for E2 activity [8,9]. In addition, ubiquitination of substrates without polymerization, mono-ubiquitination, acts as a sorting signal for protein endocytosis and as a regulation factor for diverse proteins, including histones and transcription factors [10].

In plant, genomic research of the model plant *Arabidopsis thaliana* showed that there are two E1s, 37 E2s and more than 1,300 predicted E3s [11]. Although little is known about protein ubiquitination in plants compared with yeast and mammals, recent studies revealed that the plant ubiquitination pathway is involved in the regulation of morphogenesis, the circadian clock and responding to hormone or pathogen signal molecules [12-15]. Despite the importance of ubiquitination in plants, much of the plant ubiquitination cascade is still unknown because of its complexity and the issues inherent to the use of Arabidopsis plants for biochemical analysis. Although several interactions between E2s and RING type E3s have been demonstrated *in vitro* using recombinant proteins expressed in *Escherichia coli*, these efforts are hampered by the inability to obtain functional protein using conventional methods [16].

With this in mind, we sought to develop a novel *in vitro* method to analyze the ubiquitin pathway genome-wide. The two major obstacles hindering the development of an *in vitro* assay for genome-wide screening are the difficulty of efficiently producing recombinant protein and the inability to detect ubiquitination in a high-throughput fashion. To address the first problem we used the wheat cell-free protein synthesis system, which has been previously reported to produce a wide range of functional Arabidopsis and human proteins [17-19]. Moreover, a collection of RIKEN Arabidopsis Full Length (RAFL) cDNA clones covering about 70% of Arabidopsis genes is available [20]. Using these RAFL clones as templates, recombinant proteins involved in the ubiquitination pathway were expressed in the wheat cell-free system and used for several functional analyses. For screening, conventional detection methods such as immunoblot analysis or radioisotope-labeled proteins are not suitable for the detection of a large number of ubiquitination reactions. Recently, a high-throughput luminescence method to detect protein ubiquitination was reported [21], however this method requires purified protein and creation of specialized vectors to produce proteins. In this study, a novel *in vitro* assay to detect polyubiquitin chain formation was developed using wheat cell-free synthesis and a modified luminescence-based detection method. We demonstrate (1) creation of a simple *in vitro* method to detect polyubiquitination using crude recombinant E3s, (2) discovery of the activity of At1g55530 by screening a RING subgroup in the reported assay, and (3) the polyubiquitination assay in the presence of MG132 demonstrated the absence of 26S proteasome-dependent protein degradation activity in wheat cell-free system.

Results

Detection of Polyubiquitin Chains on AtUBC22 E2 enzyme

Recently, AtUBC22 (At5g05080) E2 protein has been shown to catalyze polyubiquitin chain formation without an E3 ligase, although AtUBC35 (At1g78870) E3-independent polyubiquitination activity could not be detected [16]. We employed AtUBC22 and AtUBC35 as model E2 proteins to develop a novel polyubiquitination assay. We have also demonstrated that addition of biotin ligase (BirA) and biotin to the wheat cell-free protein production system yields a single biotinylation on a target pro-

tein containing a biotin ligation site [22]. Using this method, biotinylated recombinant AtUBC22 and AtUBC35 were synthesized and, without purification from the translation mixture, the polyubiquitination reaction was performed on the crude recombinant protein. After the reaction, biotinylated AtUBC22 and AtUBC35 were purified using streptavidin-conjugated magnetic beads and the polyubiquitin chain was detected by immunoblot analysis. As shown in Fig 1A, AtUBC22 showed polyubiquitination, whereas AtUBC35 showed mainly monoubiquitination. Interestingly, both E2s still had activity in absence of exogenous E1 in polyubiquitin reaction mixture (Fig. 1A, middle lanes), suggesting that wheat cell-free system has high endogenous E1 activity.

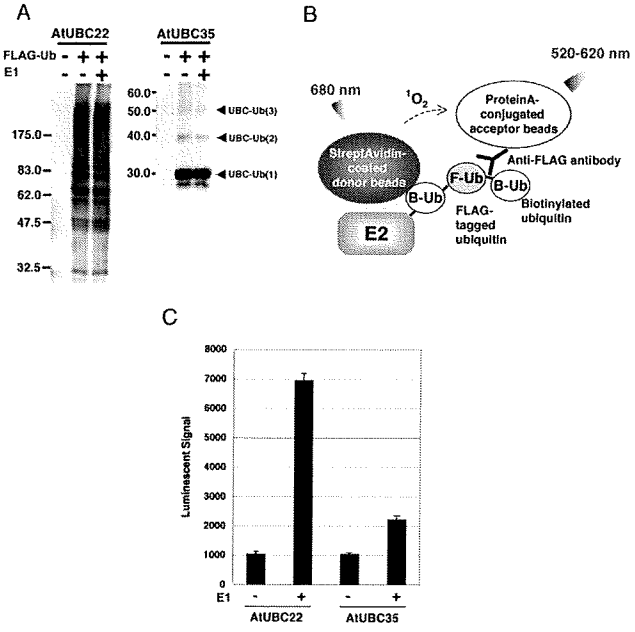

Figure 1
Detection of E3-independent polyubiquitination of AtUBC22 by luminescent analysis. A, Polyubiquitin chain on AtUBC22 but not on AtUBC35 was detected by immunoblot analysis. In this assay, polyubiquitination reaction was carried out with FLAG-tagged ubiquitin, and detected by immunoblot analysis using anti-FLAG antibody. B, Schematic diagram of detection of polyubiquitin chains by luminescent analysis. Protein A-conjugated acceptor beads and streptavidin-coated donor beads are bound to anti-FLAG antibody bound to FLAG-tagged ubiquitin and biotinylated E2, respectively, and these two beads are in closed proximity when polyubiquitin chain formed. Upon excitation 680 nm, a singlet oxygen is generated from the donor beads, and then transferred to the acceptor beads within 200 nm, and the singlet oxygen reacts the acceptor beads which in turn emits light at 520–620 nm. This light is measured by AlphaScreen kit and change to signal value. C, Polyubiquitin chain on purified recombinant E2 was detected by luminescent analysis in the presence (E1 +) or absence (E1 -) of exogenous E1. Error bars represent standard deviations from three independent experiments.

While immunoblot analysis is an excellent detection method, it is not suitable for high-throughput detection of numerous polyubiquitination reactions. Initially, we attempted to use luminescent analysis, based on the AlphaScreen technology, to detect the polyubiquitination activity of AtUBC22 and AtUBC35. In principle, if a polyubiquitin chain is formed by FLAG-tagged and biotinylated ubiquitins, it will bring into proximity the streptavidin-coated donor bead (bound to biotin) and the protein A-conjugated acceptor bead (bound to anti-FLAG IgG), producing a luminescent signal (Fig. 1B). Considering that the wheat cell-free system has high endogenous E1 activity (Fig. 1A), it may also have endogenous E2 and E3 activity. In order to avoid formation of polyubiquitin chains by an endogenous wheat germ ubiquitin pathway, purified E2s were used in this assay. As shown in Fig 1C, high luminescent signal was observed in the presence of AtUBC22 in E1-dependent manner. In contrast, AtUBC35 showed low signal. The two luminescent signals were approximately consistent with immunoblot data that AtUBC22 and AtUBC35 have high and low polyubiquitination activities respectively, as demonstrated in Fig 1A. These results indicate that the luminescent method can detect polyubiquitin chain formation by using the two types of ubiquitins.

Ubiquitination and Polyubiquitination Analyses of HECT-TypeE3 Ligases

Polyubiquitination activity of E3 ligases activated by the step-wise E1 to E3 cascade is well documented [3]. We next attempted to reconstruct this cascade *in vitro* and to detect the E3-formed polyubiquitin chains using our luminescent method. Due to the size of HECT-type E3 ligases, ranging from 100 to 428 kDa in Arabidopsis, production of active protein by traditional expression methods may not be easy and biochemical analysis using only truncated recombinant protein has been carried out previously [23]. We attempted to produce full-length Arabidopsis HECT-type E3 ligase proteins using the wheat cell-free system and monitored ubiquitin-conjugation and polyubiquitination by luminescence. Two genes that encode Arabidopsis HECT-type E3 ligase, *UPL5* and *UPL7* [24], were analyzed in this study. We obtained UPL5 and UPL7 cDNA from the RAFL library and produced FLAG-tagged protein in the wheat cell-free system. Ubiquitination of FLAG-labeled UPLs (UPL-FLAGs) was investigated by both the luminescent and immunoblot methods. The successful production of the two recombinant HECT proteins was observed by immunoblot analysis (Fig. 2A) and used in the luminescence assay without purification. To detect ubiquitination of the HECT proteins, UPL-FLAGs

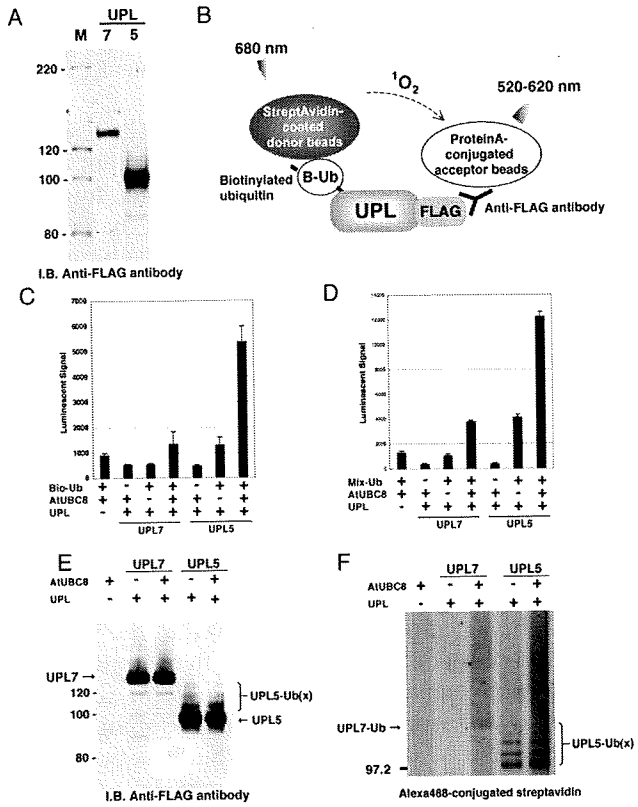

Figure 2
Analysis of recombinant Arabidopsis HECT-type E3 ligases (UPL7 and UPL5). A, Production of FLAG-tagged recombinant UPL proteins was detected by immunoblot analysis. For analysis, 5 μl of crude recombinant UPL proteins were loaded, and detected by immunoblot analysis using anti-FLAG antibody. B, Schematic diagram of detection of ubiquitin-conjugation of UPLs by luminescent analysis. Protein A-conjugated acceptor beads and streptavidin-coated donor beads were bound to anti-FLAG antibody bound to FLAG-tagged recombinant UPLs and biotinylated ubiquitin, respectively, and detected by same principle and procedure described in Figure 1B. C, The ubiquitination of crude recombinant UPL7 and UPL5 was detected by luminescent analysis described in B. Bio-Ub means biotinylated ubiquitin. D, polyubiquitination of crude recombinant UPL7 and UPL5 was detected by luminescent analysis with anti-His antibody. Mix-Ub indicated the mixture of His-tagged and biotinylated ubiquitin. E and F, Mobility shift of UPLs (E) and formation of polyubiquitin chains (F) were detected by immunoblot using anti-FLAG antibody and Alexa488-conjugated streptavidin, respectively. The polyubiquitination reaction was done with FLAG-tagged recombinant UPLs in presence or absence of crude AtUBC8, and then recombinant UPLs were purified by anti-FLAG antibody-conjugated agarose. Error bars represent standard deviations from three independent experiments.

and biotinylated ubiquitin were used. When biotinylated ubiquitin is conjugated to the UPL-FLAG, a high luminescent signal is obtained (Fig. 2B). As a result of the analysis, ubiquitin-conjugation of UPL5 was observed (Fig. 2C). In addition, polyubiquitin chains formed by UPLs were detected with the luminescence assay using His-tagged and biotinylated ubiquitin. To subtract polyubiquitin chain formation from endogenous E2 and E3 in wheat cell-free system, the assay was performed without recombinant UPL and only low signal was detected (Fig. 2D, "UPL-" lane). As expected, luminescent signal was observed in recombinant UPL5 and UPL7 (Fig. 2D). Although the luminescent signal of UPL7 was lower than that of UPL5, the signal was still two-fold higher than the endogenous background signal. These results were confirmed by immunoblot analysis that showed distinct mobility shifts of UPL5 (Fig. 2E) when detecting FLAG-tagged UPLs, and polyubiquitin chain formation of UPL5 monitoring Alexa488-conjugated streptavidin (Fig. 2F). Comparing the amount of polyubiquitin chain formation in absence of UPLs (Fig. 2F, "UPL-" lane), UPL7 formed weak but distinct polyubiquitin chains in presence of AtUBC8. These luminescent signals were consistent with immunoblot data. Interestingly, polyubiquitin chains were formed by UPL5 without supplementing exogenous E2 protein (Fig. 2D and 2F, "AtUBC8-" lane), suggesting that wheat germ extract has endogenous E2 activity as well as endogenous E1 activity. These data indicate that the wheat cell-free production system is able to produce high molecular weight proteins in functional forms and that our luminescence method can detect activity of HECT-type E3 ligases without purification. This is the first data showing that full length recombinant HECT-type E3s have ubiquitin-conjugating and polyubiquitination activity. Taken together, the luminescent method based on the wheat cell-free system could be useful for biochemical analysis of HECT-type E3 ligases.

Detection of Polyubiquitin Chains by RING-Type CIP8 E3 Ligase

It is reported that at least 469 predicted RING-type E3 ligases are encoded in the Arabidopsis genome [25]. Like the HECT-type E3, we attempted to express and carry out the functional analysis of the RING-type E3 ligases. In this study, we selected CIP8 as a model RING-type E3 ligase, which is reported to possess a RING finger motif and have typical features of an E3 ligase [26]. At first, polyubiquitination activity of purified CIP8 in presence or absence of exogenous E1 and purified E2 (AtUBC8) was investigated by luminescence. As shown in Fig 3A, luminescence analysis using His-tagged and biotinylated ubiquitin showed the polyubiquitination of purified CIP8 only when exogenous E1 and purified E2 were added to the reaction mixture. The CIP8-dependent polyubiquitination was

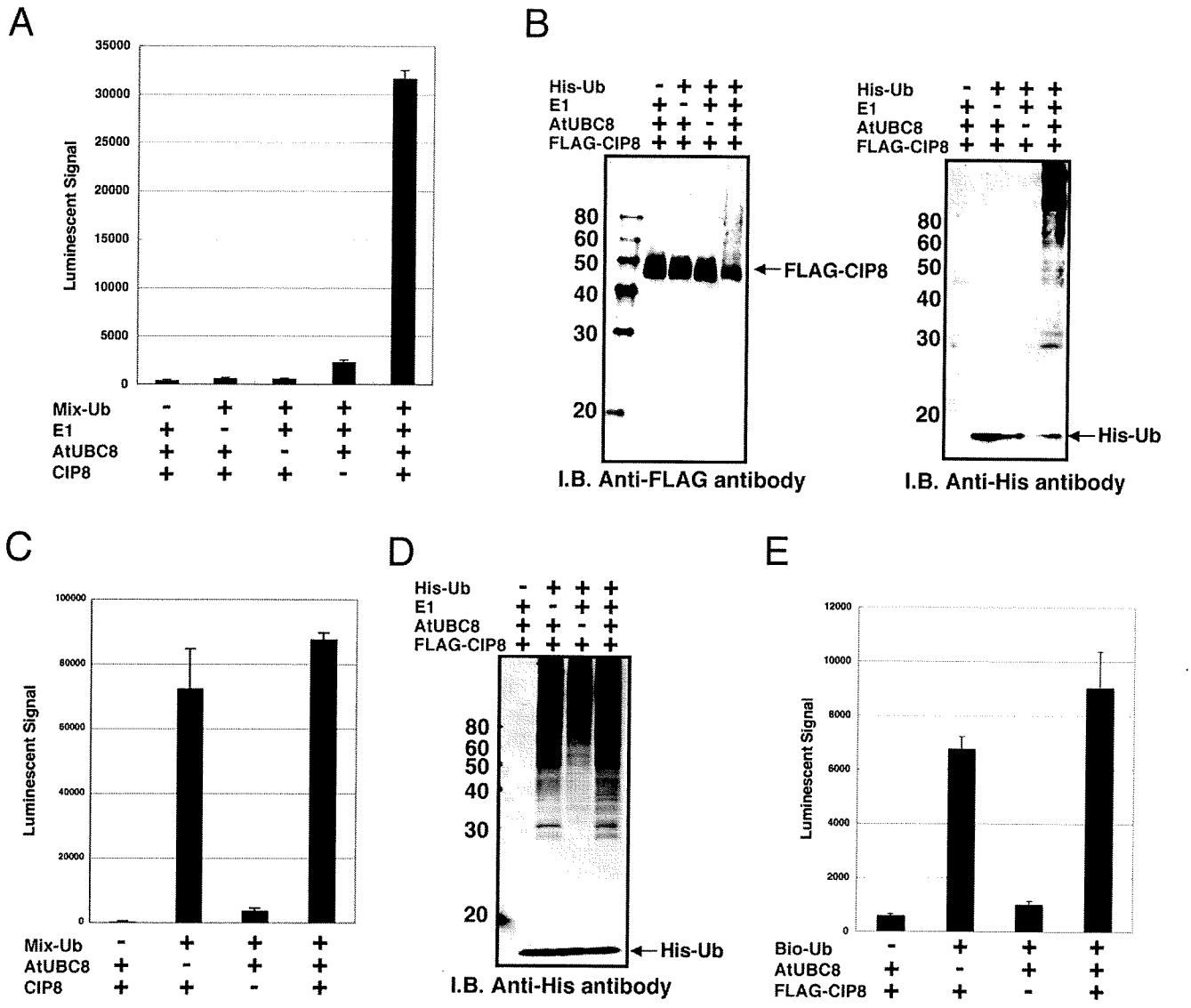

Figure 3
Detection of polyubiquitination and self-ubiquitination of CIP8. A to D, The polyubiquitination assay was carried out with purified (A and B) or crude recombinant CIP8 (C and D) and detected by luminescent analysis with anti-FLAG antibody (A and C) and immunoblot analysis (B and D). His-Ub or Mix-Ub indicate His-tagged ubiquitin or the mixture of FLAG-tagged and biotinylated ubiquitin, respectively. The polyubiquitination assay using luminescent analysis was carried out with recombinant CIP8 without tag in the presence or absence of ubiquitin related components indicated below each graph. E, Ubiquitination of crude recombinant CIP8 was observed by luminescent analysis with anti-FLAG antibody. The assay was carried out with or without biotinylated ubiquitin and crude AtUBC8 recombinant protein. Bio-Ub means biotinylated ubiquitin. Error bars represent standard deviations from three independent experiments.

confirmed by immunoblot analyses detecting both FLAG-CIP8 and His-tagged ubiquitin (Fig. 3B). On the other hand, luminescent analysis with crude CIP8 protein showed high polyubiquitination activity both in the presence or absence of purified E2 (Fig. 3C), and was confirmed by immunoblot analysis with crude protein (Fig. 3D). These data indicated that, like recombinant UPL5, crude CIP8 also utilized endogenous wheat extract E1 and E2 proteins, and therefore we could carry out the simple polyubiquitination analysis of E3 without addition of exogenous E1 and E2 proteins. Furthermore, immunoblot analysis detecting purified CIP8 (Fig. 3B) showed a mobility shift of FLAG-tagged CIP8 to higher molecular weights due to ubiquitination, whereas the mobility of the E2 was

not altered (data not shown). This result indicates that the CIP8-dependent polyubiquitin chains might be elongated on CIP8 itself. This data is consistent with a recent report showing that TRIM5a, a typical RING-type E3 ligase in human, also undergoes self-ubiquitination, forming polyubiquitin chains on itself [27]. To clarify whether the mobility shift of CIP8 was concomitant with polyubiquitin chain formation resulting from self-ubiquitination, we tried to detect ubiquitination of CIP8 by the luminescent method using crude FLAG-CIP8 protein and biotinylated ubiquitin. The luminescent method clearly detected the binding of biotinylated ubiquitin to FLAG-tagged CIP8 both in the presence and absence of exogenous E2 (Fig. 3E). Similar to polyubiquitin formation, the ubiquitination of CIP8 also occurred without the addition of exogenous E2 protein (Fig. 3E, "AtUBC8-" lane). Taken together, these data demonstrate that the luminescent method could detect formation of RING-type CIP8-dependent polyubiquitin chains and self-ubiquitination of crude CIP8.

Screening of RING-Type E3 Ligases Having Polyubiquitination Activity

Recent papers have reported that the polyubiquitin chain is an important biological regulator. Identification of activity and features of E3 ligases offers important information about the ubiquitin-dependent regulation system. Our luminescent method based on the wheat cell-free system produced a simple and high-sensitivity detection of CIP8-dependent polyubiquitin chains without any purification (Fig. 3C). Using these tools, we screened new E3 ligases for the ability to form polyubiquitin chains like CIP8.

The RING-type E3 ligases in Arabidopsis were divided into 30 subgroups based on domain structure, and CIP8 is categorized into subgroup 6 as it contains a coiled-coil domain [25]. Eight other RING-type E3s from subgroup 6 were selected for screening, and the simple polyubiquitination assay was carried out with FLAG-tagged and biotinylated ubiquitins, and the crude recombinant RING-type E3s without addition of exogenous E1 and E2. The screening result showed significant polyubiquitination activity of At1g55530, whereas other RING-E3 proteins were not active (Fig. 4A). Immunoblot analysis of purified recombinant At1g55530 confirmed the polyubiquitination activity and indicated that At1g55530 was self-ubiquitinated (Fig. 4B). The polyubiquitination activity of At1g55530 suggests that it may have a biological role for proteasome-mediated degradation like CIP8 [26]. These results show that the wheat cell-free protein expression system and the luminescent ubiquitination detection method could support functional high-throughput screening of E3 proteins.

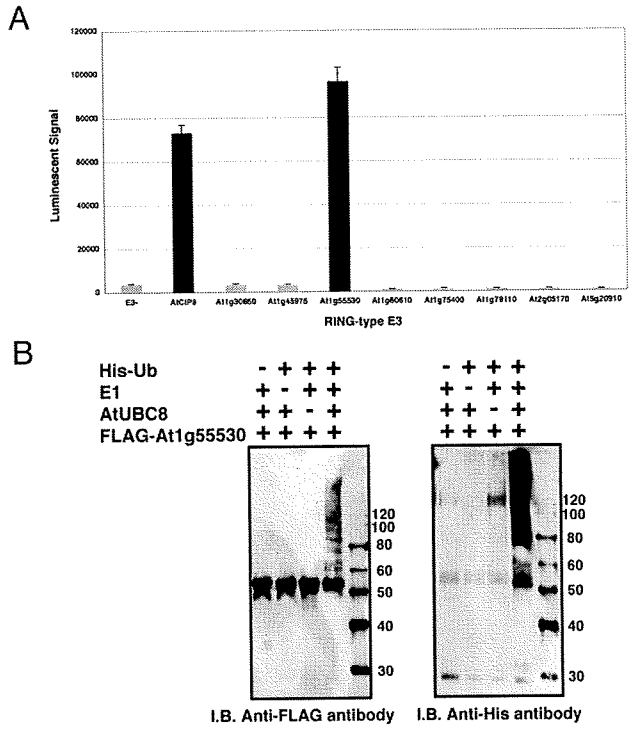

Figure 4
Screening of RING-type E3 ligases having polyubiquitination activity. A, Polyubiquitination reaction of crude recombinant E3 proteins was carried out with mixture of FLAG-tagged and biotinylated ubiquitins, and investigated by luminescent analysis with anti-FLAG antibody. B, Polyubiquitination activity of At1g55530 was confirmed by immunoblot analysis. The assay was carried out using purified recombinant AtUBC8 and At1g55530, and mobility shift of FLAG-tagged At1g55530 and polymer of His-ubiquitin were detected by immunoblot analysis using anti-FLAG and anti-His antibodies, respectively. Error bars represent standard deviations from three independent experiments.

Analysis of the Wheat Cell-free Based Ubiquitination in the Presence of Proteasome Inhibitor

It is known that some cell extracts, such as rabbit reticulocyte or HeLa S-100 fraction, have 26S proteasome-dependent proteolytic activity [28,29]. Based on the presence of endogenous E1 and E2 ubiquitination and polyubiquitination in the wheat cell-free system, it is expected that the 26S proteasome activity will be very low (Fig. 2, 3 and 4). It was previously reported that the wheat germ extract had little 26S proteasome-dependent protein degradation activity [30]. Thus, we determined whether the wheat cell-free system contains active 26S proteasome. Using the crude recombinant proteins that formed polyubiquitin chains in this study, the polyubiquitination reaction was carried out in presence or absence of MG132, and accrual of the polyubiquitinated recombinant pro-

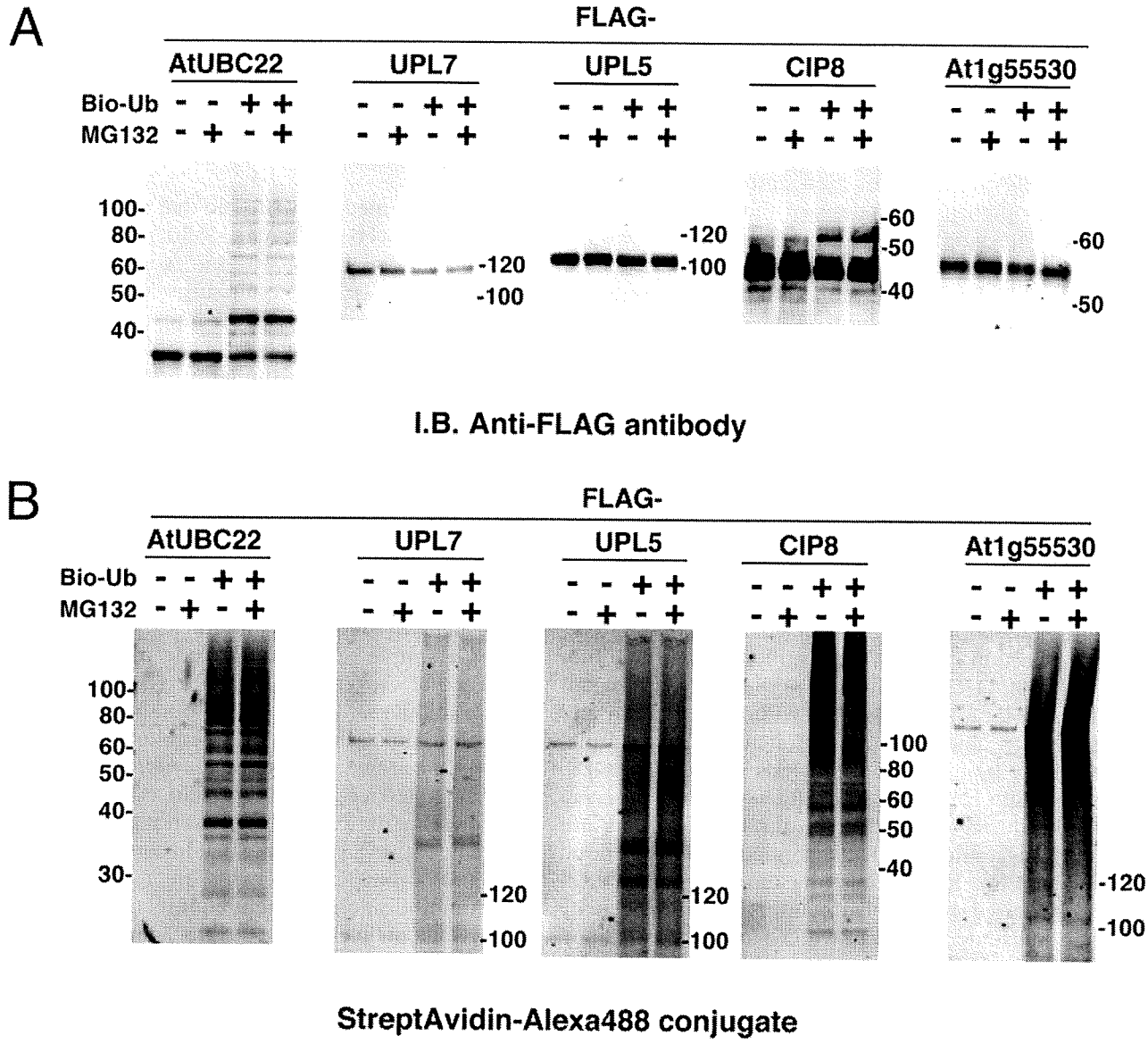

Figure 5
Effect of proteasome inhibitor on stability of polyubiquitinated proteins. Polyubiquitination assays of crude FLAG-tagged E2s and E3s were carried out in the presence or absence of biotinylated ubiquitin and 20 μM MG132. A, FLAG-tagged recombinant proteins were detected by immunoblot analysis using anti-FLAG antibody. B, Polyubiquitination chain formed by each recombinant protein was detected by Alexa488-conjugated streptavidin.

teins and its polyubiquitin chain was estimated. As shown in Fig 5, the amounts of UBC22, UPL5, UPL7 and At1g55530 (Fig. 5A) and of its polyubiquitin chains (Fig. 5B) were hardly altered by MG132 treatment. This result indicates that the proteolytic activity of the 26S proteasome in the wheat cell-free system was below the detection level. Thus, the wheat cell-free system could be suitable for ubiquitination analysis.

Discussion

The ubiquitin signal is an important protein modification in eukaryotes. Binding of a single ubiquitin to a target protein, mono-ubiquitination, is essential for membrane trafficking, protein functions and protein-protein interaction [7]. As for polyubiquitination, both Lys-48- and Lys-63-linked polyubiquitin chains have been well characterized in mammals and yeast. Lys-48 linked chains cause proteolysis of target proteins [6], and Lys-63 linked chains reg-

ulate signal transduction such as cellular localization of protein or protein-protein interactions [7]. In mammals, the multi-functional activities of NF-κB are regulated by the Lys-63 linked chain [31]. In plants, the function of the Lys-63 linked chain is still obscure. However, Arabidopsis E2 and its variants promote formation of the Lys-63 linked chain [32], suggesting that the Lys-63 linked chain in plant cells might also function similar to animal cells. Hence, comprehensive analysis of the ubiquitin-related plant proteins would open a door for elucidation of the plant ubiquitin pathway. In this study, we developed a simple and highly sensitive ubiquitination assay method by combination of the wheat cell-free protein synthesis system and luminescent detection. In general, *in vivo* protein production requires many time-consuming steps such as vector construction, cell culture and purification to obtain the recombinant protein. In contrast, this cell-free based luminescence method could analyze a large amount of ubiquitin reactions without these steps.

Using this method, we conveniently detected polyubiquitin chain formation of E2 and E3s by using two tagged ubiquitins (Fig. 1, 2, 3 and 4). The result of polyubiquitination analysis of the E2s obtained from luminescent-based detection method was verified by immunoblot analysis (Fig. 1). Our analysis also produced recombinant protein of HECT-type E3 ligases without truncation and detected their ubiquitin-conjugation and polyubiquitination activity by luminescent analysis (Fig. 2C and 2D). The ubiquitin-conjugation of UPL5 was not observed when a reductant was added to the reaction (data not shown), suggesting that UPL5 formed a thioester bond with ubiquitin. In addition, the model RING-type E3 CIP8 possessed high polyubiquitin formation activity without substrate, consistent with what was reported previously [26]. Crude recombinant CIP8 formed polyubiquitin chains in the absence of exogenous E1 and E2 (Fig. 3C and 3D), suggesting that the wheat cell-free system might include enough endogenous E1 and E2 activity. It was reported that wheat germ extracts have only a partial ubiquitin pathway [30]. Although the process to isolate wheat germ extract is different from the conventional methods [33], this report strongly supports the existence of endogenous ubiquitin pathway in our wheat cell-free system. Indeed, luminescent analysis using crude recombinant protein showed slight polyubiquitin chain formation even in absence of recombinant E3 (Fig. 2D, Fig. 3C and Fig. 4A, "E3-" lane), indicating that wheat cell-free system might include not only E1 and E2, but E3s or other factors that accelerates the polyubiquitin chain formation. Further, quantitative immunoblot analysis using anti-ubiquitin antibody showed that free ubiquitin was also present in wheat germ extract at a concentration of at least 10 nM (data not shown). This is similar to the ubiquitin concentration supplied in the *in vitro* assay. Although we developed a convenient screening method to detect E3 activity in this study, removal of the endogenous ubiquitin and ubiquitin related components such as E1, E2 and E3, would yield a more sensitive assay. However, wheat cell-free system does not have 26S proteasome proteolytic activity (Fig. 5), indicating that using crude recombinant protein is sufficient for *in vitro* ubiquitination assays.

By using this method, we found that a previously uncharacterized RING type E3, At1g55530, possessed high polyubiquitination activity without exogenous E1 and E2 proteins (Fig. 4). This result suggested that the method developed here is expected to find the activity of other unknown E3 ligases such as At1g55530. Despite having only 32% sequence similarity, the E3s CIP8 and At1g55530 showed similar biochemical functions. Polyubiquitin chains formed by CIP8 and At1g55530 elongated on themselves, while another report showed that polyubiquitin chains were formed on E2 before transferring them to substrates [34]. This reflects that the pattern of polyubiquitin chain formation differs between individual E3s and that the detailed mechanisms are still unknown. These studies suggest the importance of functional analysis using active recombinant proteins. Although we developed a simple screen using crude recombinant E3s in absence of exogenous E1 and E2 (Fig. 4), this method could not detect the activity of some E3 ligases that were unable to utilize endogenous ubiquitination components in wheat cell-free system. The polyubiquitination activity of At5g20910 recombinant protein, expressed in *E. coli* in the presence of AtUBC8 [25], was not active in our *in vitro* system (Fig. 4A), suggesting that in some cases exogenous E2 and/or other components are necessary additions. Such modifications to the ubiquitination assays detailed here would help elucidate the biochemical features of E3s (e.g., addition of recombinant E2s to reaction mixture could give us further information about the E2–E3 specificity, and of other E3 components would lead to the elucidation of structure of complex type E3 ligase such as SCF).

Conclusion

In this study, we found that the wheat cell-free system was an excellent expression system to produce recombinant protein efficiently and to carry out *in vitro* ubiquitination assays without the interference of proteolytic activity. Coupled with luminescent analysis, detection of these ubiquitin reactions in the crude translation reaction mixture was possible. Thus, this method should be helpful for solving the complicated ubiquitin pathway in plant.

Methods

Construction of DNA Templates for Transcription

We used RAFL as templates. DNA templates of E2s and E3s for transcription were constructed by "Split-Primer"

PCR as described previously [17]. Primers used in this study are summarized in Additional file 1. The first round of PCR was performed on each cDNA template using 10 nM of each of the following primers: a target protein specific primer (5'-CCACCCACCACCACCAatgnnnnnnnnn nnnnnnnn-3'; lowercase indicates the 5'-coding region of the target gene) and the AODA2306 primer. Then, a second round of PCR was carried out to construct the templates for protein synthesis using a portion (5 μl) of the first PCR mix, 100 nM SPu primer, 100 nM AODA2303 primer and 1 nM deSP6E02 primer. GST tags were used according to the methods we described previously [17]. The transcription templates of two HECT-type E3 ligases, UPL7 and UPL5, were generated as C-terminal FLAG-tagged proteins using the Gateway System® (Invitrogen, Carlsbad, CA, USA). Briefly, the ORF sequences of UPL7 and UPL5 were amplified by PCR with sense and antisense primers containing attB1 and FLAG-attB2 sequences, respectively. According to the manufacturer's instructions (Invitrogen), these DNA fragments were subcloned into pDONR221 vector by BP reaction and then inserted into the Gateway-based pEU vector (pEU-E01-GW) by LR reaction. Using these recombinant vectors as templates, PCR was carried out with 100 nM SPu primer and 100 nM AODA2303 primer and used as transcription templates.

Cell-free Protein Synthesis

In vitro transcription and cell-free protein synthesis were performed as described [18]. Transcript was made from each of the DNA templates mentioned above using the SP6 RNA polymerase. The synthetic mRNAs were then precipitated with ethanol and collected by centrifugation using a Hitachi R10H rotor. Each mRNA (usually 30–35 μg) was washed and transferred into a translation mixture. The translation reaction was performed in the bilayer mode [35] with slight modifications. The translation mixture that formed the bottom layer consisted of 60 A260 units of the wheat germ extract (CellFree Sciences, Yokohama, Japan) and 2 μg creatine kinase (Roche Diagnostics K. K., Tokyo, Japan) in 25 μl of SUB-AMIX® (CellFree Sciences). The SUB-AMIX® contained (final concentrations) 30 mM Hepes/KOH at pH 8.0, 1.2 mM ATP, 0.25 mM GTP, 16 mM creatine phosphate, 4 mM DTT, 0.4 mM spermidine, 0.3 mM each of the 20 amino acids, 2.7 mM magnesium acetate, and 100 mM potassium acetate. SUB-AMIX® (125 μl) was placed on the top of the translation mixture, forming the upper layer. After incubation at 16°C for 15 h, the synthesized proteins were confirmed by SDS-PAGE. For biotin labeling, 1 μl of crude biotin ligase (BirA) produced by the wheat cell-free expression system was added to the bottom layer, and 0.5 μM (final concentration) of D-biotin (Nacalai Tesque, Inc., Kyoto, Japan) was added to both upper and bottom layers, as described previously [22].

Purification of E2 and E3 Proteins

Purification of GST-tagged protein was carried out according to the procedure described previously [36] with slight modification. Crude GST-tagged recombinant protein (450 μl) produced by the cell-free reaction was precipitated with glutathione sepharose™ 4B (GE Healthcare, Buckinghamshire, UK). The recombinant proteins were eluted with PBS buffer containing 0.1 U of AcTEV protease (Invitrogen) in order to cleave the GST tag from the protein.

Detection of Polyubiquitination by the Luminescent Method

In vitro polyubiquitination assays were carried out in a total volume of 15 μl consisting of 20 mM Tris-HCl pH 7.5, 0.2 mM DTT, 5 mM $MgCl_2$, (10 μM zinc acetate in the assays for RING-type E3s only), 3 mM ATP, 1 mg/ml BSA, 25 nM biotinylated ubiquitin, 25 nM FLAG-tagged ubiquitin, 1 μl of recombinant E2 (purified or crude) and 1 μl of recombinant E3 (purified or crude) in the presence or absence of 0.05 μM rabbit E1 (Boston Biochem, Cambridge, MA, USA) at 30°C for 1 hr in a 384-well Optiplate (PerkinElmer, Boston, MA, USA). In accordance with the AlphaScreen IgG (ProteinA) detection kit (Perkin Elmer) instruction manual, 10 μl of detection mixture containing 20 mM Tris-HCl pH 7.5, 0.2 mM DTT, 5 mM $MgCl_2$, 5 μg/ml Anti-FLAG antibody (Sigma-Aldrich, St. Louis, MO, USA), 1 mg/ml BSA, 0.1 μl streptavidin-coated donor beads and 0.1 μl anti-IgG acceptor beads were added to each well of the 384 Optiplate followed by incubation at 23°C for 1 hr. Luminescence was analyzed by the AlphaScreen detection program.

Detection of Ubiquitinated E2 by Immunoblot Analysis

Crude biotinylated recombinant E2 proteins (40 μl) were used for the ubiquitin-conjugating assay in a total reaction volume of 50 μl containing 20 mM Tris-HCl pH 7.5, 0.2 mM DTT, 5 mM $MgCl_2$, 3 mM ATP and 4 μM FLAG-tagged ubiquitin (Sigma) for 3 hr at 30°C. The reaction products were purified by Streptavidin Magnesphere Paramagnetics particles (Promega, Madison, WI, USA). After washing the beads with PBS buffer, recombinant E2s were boiled in 15 μl of SDS sample buffer containing 50 mM Tris-HCl pH 6.8, 2% SDS, 10% glycerol and 0.2% bromophenol blue, and then separated from the magnet beads. The proteins were separated by SDS-PAGE and transferred to PVDF membrane (Millipore Bedford, MA, USA) according to standard procedures. The blots were detected by the ECL plus detection system (GE Healthcare) with anti-FLAG antibody (Sigma) according to the manufacturer's procedure.

Detection of Polyubiquitination by the Immunoblot Analysis

For polyubiquitination of HECT-type E3 ligases, crude FLAG-tagged UPL recombinant protein (20 μl) was ubiq-

uitinated in a total reaction volume of 50 μl consisting of 20 mM Tris-HCl pH 7.5, 0.2 mM DTT, 5 mM $MgCl_2$, 3 mM ATP, 4 μM biotinylated ubiquitin and 20 μl of crude recombinant AtUBC8 for 3 hr at 30°C. Then, recombinant UPL protein was gathered by anti-FLAG M2 agarose (Sigma). After washing the agarose with PBS buffer, the recombinant UPL protein was boiled in 15 μl of SDS sample buffer and then separated from beads by centrifugation. For polyubiquitination of RING-type E3 ligases, the assay was carried out in 10 μl of reaction mixture containing 20 mM Tris-HCl pH 7.5, 0.2 mM DTT, 5 mM $MgCl_2$, 10 μM zinc acetate, 3 mM ATP, 1 mg/ml BSA, 4 μM FLAG- or His-tagged ubiquitin, 1 μl of purified or crude recombinant E2 and 1 μl of purified or crude recombinant E3 at 30°C for 3 hr. Then, 5 μl of three-fold concentrated SDS sample buffer was added to the reaction mixture and boiled for 5 min. Proteins were separated by SDS-PAGE and transferred to Hybond-LFP PVDF membrane (GE Healthcare) according to standard procedures. Immunoblot analysis was carried out with anti-FLAG antibody (Sigma) or anti-His antibody (GE Healthcare) according to the procedure described above. When detecting biotinylated ubiquitin, blots were treated with 5 μg/ml Alexa488-conjugated streptavidin (Invitrogen) in PBS buffer. After washing with PBS containing 0.1% Tween-20, the blot was analyzed by a Typhoon Imager (GE Healthcare) using the 532 nm laser and 526 emission filters.

Polyubiquitination Assay with 26S Proteasome Inhibitor

Polyubiquitination reaction was carried out as same procedure described above except addition of MG132 (Calbiochem, San Diego, CA, USA) at a final concentration of 20 μM to reaction mixture. Then, the protein on blot was detected by immunoblot analysis with anti-FLAG antibody or Alexa488-conjugated streptavidin.

Authors' contributions

HT conceived the study and performed the experiments, and contributed to writing the manuscript. MS and KS provided RAFL cDNA clones. AN conceived the study. YE conceived the study and supervised the work. TS conceived and designed the study, supervised the work and contributed to writing the manuscript.

Additional material

Additional file 1

AGI code of Arabidopsis genes and primer sequences used in this study.

AGI code of Arabidopsis genes and primer sequences used in this study. Click here for file [http://www.biomedcentral.com/content/supplementary/1471-2229-9-39-S1.xls]

Acknowledgements

This work was partially supported by the Special Coordination Funds for Promoting Science and Technology by the Ministry of Education, Culture, Sports, Science and Technology, Japan (T. S. and Y. E.). We thank Michael Andy Goren for proofreading this manuscript.

References

1. Bai C, Sen P, Hofmann K, Ma L, Goebl M, Harper JW, Elledge SJ: **SKP1 Connects Cell Cycle Regulators to the Ubiquitin Proteolysis Machinery through a Novel Motif, the F-Box.** *Cell* 1996, **86(2)**:263-274.
2. Chen Z, Hagler J, Palombella VJ, Melandri F, Scherer D, Ballard D, Maniatis T: **Signal-induced site-specific phosphorylation targets IκBα to the ubiquitin-proteasome pathway.** *Genes Dev* 1995, **9(13)**:1586-1597.
3. Pickart CM: **Mechanisms underlying ubiquitination.** *Annu Rev Biochem* 2001, **70**:503-533.
4. Smalle J, Vierstra RD: **The ubiquitin 26S proteasome proteolytic pathway.** *Annu Rev Plant Biol* 2004, **55**:555-590.
5. Borden KL: **RING domains: master builders of molecular scaffolds?** *J Mol Biol* 2000, **295(5)**:1103-1112.
6. Glickman MH, Ciechanover A: **The ubiquitin-proteasome proteolytic pathway: destruction for the sake of construction.** *Physiol Rev* 2002, **82(2)**:373-428.
7. Schnell JD, Hicke L: **Non-traditional functions of ubiquitin and ubiquitin-binding proteins.** *J Biol Chem* 2003, **278(38)**:35857-35860.
8. Hofmann RM, Pickart CM: **Noncanonical MMS2-encoded ubiquitin-conjugating enzyme functions in assembly of novel polyubiquitin chains for DNA repair.** *Cell* 1999, **96(5)**:645-653.
9. Yin XJ, Volk S, Ljung K, Mehlmer N, Dolezal K, Ditengou F, Hanano S, Davis SJ, Schmelzer E, Sandberg G, Teige M, Palme K, Pickart C, Bachmair A: **Ubiquitin lysine 63 chain forming ligases regulate apical dominance in Arabidopsis.** *Plant Cell* 2007, **19(6)**:1898-1911.
10. Hicke L: **A new ticket for entry into budding vesicles – ubiquitin.** *Cell* 2001, **106(5)**:527-530.
11. Vierstra RD: **The ubiquitin/26S proteasome pathway, the complex last chapter in the life of many plant proteins.** *Trends Plant Sci* 2003, **8(3)**:135-142.
12. Nelson DC, Lasswell J, Rogg LE, Cohen MA, Bartel B: **FKF1, a Clock-Controlled Gene that Regulates the Transition to Flowering in Arabidopsis.** *Cell* 2000, **101(3)**:331-340.
13. Osterlund MT, Hardtke CS, Wei N, Deng XW: **Targeted destabilization of HY5 during light-regulated development of Arabidopsis.** *Nature* 2000, **405(6785)**:462-466.
14. Stone SL, Williams LA, Farmer LM, Vierstra RD, Callis J: **KEEP ON GOING, a RING E3 ligase essential for Arabidopsis growth and development, is involved in abscisic acid signaling.** *Plant Cell* 2006, **18(12)**:3415-3428.
15. Rosebrock TR, Zeng L, Brady JJ, Abramovitch RB, Xiao F, Martin GB: **A bacterial E3 ubiquitin ligase targets a host protein kinase to disrupt plant immunity.** *Nature* 2007, **448(7151)**:370-374.
16. Kraft E, Stone SL, Ma L, Su N, Gao Y, Lau OS, Deng XW, Callis J: **Genome analysis and functional characterization of the E2 and RING-type E3 ligase ubiquitination enzymes of Arabidopsis.** *Plant Physiol* 2005, **139(4)**:1597-1611.
17. Sawasaki T, Ogasawara T, Morishita R, Endo Y: **A cell-free protein synthesis system for high-throughput proteomics.** *Proc Natl Acad Sci USA* 2002, **99(23)**:14652-14657.
18. Sawasaki T, Gouda MD, Kawasaki T, Tsuboi T, Tozawa Y, Takai K, Endo Y: **The wheat germ cell-free expression system: methods for high-throughput materialization of genetic information.** *Methods Mol Biol* 2005, **310**:131-144.
19. Kobayashi T, Kodani Y, Nozawa A, Endo Y, Sawasaki T: **DNA-binding profiling of human hormone nuclear receptors via fluorescence correlation spectroscopy in a cell-free system.** *FEBS Lett* 2008, **582(18)**:2737-2744.
20. Seki M, Narusaka M, Kamiya A, Ishida J, Satou M, Sakurai T, Nakajima M, Enju A, Akiyama K, Oono Y, Muramatsu M, Hayashizaki Y, Kawai J, Carninci P, Itoh M, Ishii Y, Arakawa T, Shibata K, Shinagawa A, Shinozaki K: **Functional annotation of a full-length Arabidopsis cDNA collection.** *Science* 2002, **296(5565)**:141-145.
21. Kus B, Gajadhar A, Stanger K, Cho R, Sun W, Rouleau N, Lee T, Chan D, Wolting C, Edwards A, Bosse R, Rotin D: **A high throughput**

screen to identify substrates for the ubiquitin ligase Rsp5. *J Biol Chem* 2005, **280(33)**:29470-29478.
22. Sawasaki T, Kamura N, Matsunaga S, Saeki M, Tsuchimochi M, Morishita R, Endo Y: **Arabidopsis HY5 protein functions as a DNA-binding tag for purification and functional immobilization of proteins on agarose/DNA microplate.** *FEBS Lett* 2008, **582(2)**:221-228.
23. Bates PW, Vierstra RD: **UPL1 and 2, two 405 kDa ubiquitin-protein ligases from Arabidopsis thaliana related to the HECT-domain protein family.** *Plant J* 1999, **20(2)**:183-195.
24. Downes BP, Stupar RM, Gingerich DJ, Vierstra RD: **The HECT ubiquitin-protein ligase (UPL) family in Arabidopsis: UPL3 has a specific role in trichome development.** *Plant J* 2003, **35(6)**:729-742.
25. Stone SL, Hauksdóttir H, Troy A, Herschleb J, Kraft E, Callis J: **Functional analysis of the RING-type ubiquitin ligase family of Arabidopsis.** *Plant Physiol* 2005, **137(1)**:13-30.
26. Hardtke CS, Okamoto H, Deng XW: **Biochemical evidence for ubiquitin ligase activity of the Arabidopsis COP1 interacting protein 8 (CIP8).** *Plant J* 2002, **30(4)**:385-394.
27. Yamauchi K, Wada K, Tanji K, Tanaka M, Kamitani T: **Ubiquitination of E3 ubiquitin ligase TRIMa and its potential role.** *FEBS J* 2008, **275(7)**:1540-1555.
28. Waxman L, Fagan JM, Goldberg AL: **Demonstration of two distinct high molecular weight proteases in rabbit reticulocytes, one of which degrades ubiquitin conjugates.** *J Biol Chem* 1987, **262(6)**:2451-2457.
29. Chen ZJ, Parent L, Maniatis T: **Site-Specific Phosphorylation of IκBα by a Novel Ubiquitination-Dependent Protein Kinase Activity.** *Cell* 1996, **84(6)**:853-862.
30. Hatfield PM, Vierstra RD: **Ubiquitin-dependent proteolytic pathway in wheatgerm: Isolation of multiple forms of ubiquitin-activating enzyme, E1.** *Biochemistry* 1989, **28**:735-742.
31. Wu CJ, Conze DB, Li T, Srinivasula SM, Ashwell JD: **Sensing of Lys 63-linked polyubiquitination by NEMO is a key event in NF-κB activation.** *Nature Cell Biol* 2006, **8(4)**:398-406.
32. Yin XJ, Volk S, Ljung K, Mehlmer N, Dolezal K, Ditengou F, Hanano S, Davis SJ, Schmelzer E, Sandberg G, Teige M, Palme K, Pickart C, Bachmaira A: **Ubiquitin lysine 63 chain-forming ligases regulate apical dominance in Arabidopsis.** *Plant Cell* 2007, **19(6)**:1898-1911.
33. Madin K, Sawasaki T, Ogasawara T, Endo Y: **A highly efficient and robust cell-free protein synthesis system prepared from wheat embryos: Plants apparently contain a suicide system directed at ribosomes.** *Proc Natl Acad Sci USA* 2000, **97(2)**:559-564.
34. Li W, Tu D, Brunger AT, Ye Y: **A ubiquitin ligase transfers preformed polyubiquitin chains from a conjugating enzyme to a substrate.** *Nature* 2007, **446(7133)**:333-337.
35. Sawasaki T, Hasegawa Y, Tsuchimochi M, Kamura N, Ogasawara T, Kuroita T, Endo Y: **A bilayer cell-free protein synthesis system for high-throughput screening of gene products.** *FEBS Lett* 2002, **514(1)**:102-105.
36. Masaoka T, Nishi M, Ryo A, Endo Y, Sawasaki T: **The wheat germ cell-free based screening of protein substrates of calcium/calmodulin-dependent protein kinase II delta.** *FEBS Lett* 2008, **582(13)**:1795-1801.

THE JOURNAL OF BIOLOGICAL CHEMISTRY VOL. 284, NO. 42, pp. 28642–28649, October 16, 2009

Paraquat Toxicity Induced by Voltage-dependent Anion Channel 1 Acts as an NADH-dependent Oxidoreductase*[S]

Received for publication, June 12, 2009, and in revised form, August 7, 2009 Published, JBC Papers in Press, August 28, 2009, DOI 10.1074/jbc.M109.033431

Hiroki Shimada[‡1], Kei-Ichi Hirai[§], Eriko Simamura[‡], Toshihisa Hatta[‡], Hiroki Iwakiri[¶], Keiji Mizuki[¶], Taizo Hatta[¶], Tatsuya Sawasaki[‖], Satoko Matsunaga[‖], Yaeta Endo[‖**], and Shigeomi Shimizu[‡‡]**

*From [‡]Molecular and Cell Structural Science, Kanazawa Medical University, Uchinada, Ishikawa 920-0293, the [§]Niwa Institute for Immunology, Tosashimizu, Kochi 787-0306, the [¶]Department of Nanoscience, Sojo University, Ikeda, Kumamoto 860-0082, the [‖]Cell-free Science and Technology Research Center and the Venture Business Laboratory, Ehime University, Matsuyama, Ehime 790-8577, the **RIKEN Genomic Sciences Center, Tsurumi, Yokohama 230-0045, and the [‡‡]Department of Pathological Cell Biology, Medical Research Institute, Tokyo Medical and Dental University, Yushima, Bunkyo, Tokyo 113-8510, Japan*

Paraquat (PQ), a herbicide used worldwide, causes fatal injury to organs upon high dose ingestion. Treatments for PQ poisoning are unreliable, and numerous deaths have been attributed inappropriate usage of the agent. It is generally speculated that a microsomal drug-metabolizing enzyme system is responsible for PQ toxicity. However, recent studies have demonstrated cytotoxicity via mitochondria, and therefore, the cytotoxic mechanism remains controversial. Here, we demonstrated that mitochondrial NADH-dependent PQ reductase containing a voltage-dependent anion channel 1 (VDAC1) is responsible for PQ cytotoxicity. When mitochondria were incubated with NADH and PQ, superoxide anion ($O_2^{\cdot-}$) was produced, and the mitochondria ruptured. Outer membrane extract oxidized NADH in a PQ dose-dependent manner, and oxidation was suppressed by VDAC inhibitors. Zymographic analysis revealed the presence of VDAC1 protein in the oxidoreductase, and the direct binding of PQ to VDAC1 was demonstrated using biotinylated PQ. VDAC1-overexpressing cells showed increased $O_2^{\cdot-}$ production and cytotoxicity, both of which were suppressed in VDAC1 knockdown cells. These results indicated that a VDAC1-containing mitochondrial system is involved in PQ poisoning. These insights into the mechanism of PQ poisoning not only demonstrated novel physiological functions of VDAC protein, but they may facilitate the development of new therapeutic approaches.

Paraquat (PQ[2]; methyl viologen, 1,1′-dimethyl-4,4′-bipyridinium dichloride) is an effective herbicide used in more than 120 countries (1). Although it is classified as a low hazard compound, PQ is hazardous when used improperly and has been found responsible for thousands of deaths worldwide because of intentional overdose and high levels of occupational and accidental exposure especially in developing countries (1). Direct exposure to PQ causes severe irritation to the eyes and skin, and ingestion of concentrated products may result in fatal injury to lungs because of edema, hemorrhage, and subsequent fibrosis as well as damage to other organs (2). Additionally, PQ has emerged as a risk factor for Parkinson disease (3). The acute toxicity of PQ in mammals is mediated by reactive oxygen species (ROS) produced by a cyclic oxidation-reduction reaction (4). It is generally speculated that NADPH-cytochrome P450 reductase in microsomal drug-metabolizing enzyme systems is responsible for the production of ROS (5). However, we previously observed that the initial ultrastructural alterations associated with PQ exposure occurred only in mitochondria and not in the endoplasmic reticulum in pulmonary cells *in vivo* (6) and *in vitro* (7). In addition, several reports have suggested the cytotoxicity of PQ via mitochondrial dysfunction (8–10). Despite the development of a number of treatments for PQ poisoning, the efficacy and reliability of currently available treatments have remained limited because of an insufficient understanding of PQ cytotoxicity (2).

We recently discovered that active NADH-dependent oxidoreductase located on the mitochondrial outer membrane reduced PQ to a radical form that spontaneously formed superoxide anion ($O_2^{\cdot-}$) and destroyed mitochondria (11–13). Furthermore, we demonstrated that 1) PQ was initially metabolized to monopyridone in the cytosol and subsequently hydroxylated by the microsomes and 2) the induction of drug-metabolizing enzymes and the administration of a ROS scavenger reduced PQ toxicity in mice (11, 14). These results indicate that the mitochondrial system, not the microsomal system, is responsible for PQ toxicity. We verified that enzymes in the electron transport chain and NADH-cytochrome b_5 reductase, an NADH-dependent oxidoreductase in the outer membrane, were not involved in this reaction (11, 12). A voltage-dependent anion channel (VDAC), an abundant pore-forming protein in the outer membrane, exerts numerous physiological functions as a channel; it regulates both the metabolite flux of mitochondria and transmembrane potential, and plays a role in apoptosis. Recently, it was reported that NADH regulates VDAC func-

* This work was supported by Grants-in-aid for Scientific Research 15591664, 17591899, 19390291, and 21791045 from the Japan Society for the Promotion of Science, Grants for Promoted Research S2003-12, S2004-12, C2007-4, S2007-9, C2008-1, S2008-10, C2009-3, and S2009-10 from Kanazawa Medical University, Grant for Project Research H2009-14 from High-Tech Research Center of Kanazawa Medical University, and in part by The Ministry of Education, Culture, Sports, Science, and Technology, Japan Grant S0801085.

[S] The on-line version of this article (available at http://www.jbc.org) contains supplemental schemes.

[1] To whom correspondence should be addressed. Fax: 81-76-218-8189; E-mail: simada-h@kanazawa-med.ac.jp.

[2] The abbreviations used are: PQ, paraquat; BQ, benzoquinone; DCF, 2′,7′-dichlorofluorescein; DCFH, DCF-diacetate; DIDS, 4,4′-diisothiocyanatostilbene-2,29-disulfic acid; IC_{50}, 50% growth inhibition toxicity; mAb, monoclonal antibody; PTP, permeability transition pore; TBS, Tris-buffered saline; VDAC, voltage-dependent anion channel; ROS, reactive oxygen species; SOD, superoxide dismutase; siRNA, small Interfering RNA.

tion (15), and an isoform of VDAC localized in the plasma membrane possesses NADH-ferricyanide reductase activity (16). Therefore, we attempted to determine whether or not NADH-PQ oxidoreductase on mitochondria is responsible for PQ cytotoxicity and if VDAC participates in this activity.

EXPERIMENTAL PROCEDURES

Cell Line

HeLa cells were provided by RIKEN Cell Bank (Tsukuba, Japan). Cells were cultured in Dulbecco's modified Eagle's medium (Sigma-Aldrich) supplemented with 10% fetal bovine serum at 37 °C in a humidified CO_2 incubator.

Intracellular ROS Production

Mitochondrial superoxide production in HeLa cells was detected using MitoSOX® (Molecular Probes Inc., Eugene, OR), a red fluorescent mitochondrial superoxide indicator, according to the given protocol. Cells were pretreated with 1 mM PQ; Sigma-Aldrich) for 50 min at 37 °C and incubated with 5 μM MitoSOX for 10 min in the dark. The medium was exchanged for fresh medium, and the cells were observed by a fluorescence microscope (Olympus IX70, Olympus Corp., Tokyo, Japan). The effects of benzoquinone (BQ; 0.2 mM, Sigma-Aldrich) were evaluated after 10 min of incubation in BQ-added medium. Intracellular H_2O_2 production in HeLa cells by PQ was detected using 2′,7′-dichlorofluorescein-diacetate (DCFH; Molecular Probes) (17, 18). Briefly, cells were pretreated with 1 mM PQ for 1 h at 37 °C, and then the cells were incubated with 5 μM DCFH for 20 min in the dark. Afterward, the medium was exchanged for fresh medium; fluorescence images that appeared after the formation of 2′,7′-dichlorofluorescein (DCF) were observed by fluorescence microscopy.

Preparation of Mitochondria

Mitochondria were isolated from the livers of male Wistar rats or from HeLa cells by differential centrifugation (11, 12). Mitochondria were suspended in 0.25 M sucrose solution containing 0.05 M Tris-HCl, 20 mM KCl, 2.0 mM $MgCl_2$, and 1.0 mM Na_2HPO_4 (pH 7.4). The mitochondria were starved for 20 min at 37 °C to consume endogenous substrates before use. The Kanazawa Medical University Animal Care and Use Committee approved all studies. All animals were cared for and treated in accordance with the Committee guidelines.

PQ-dependent Hydrogen Peroxide (H_2O_2) Production on Mitochondria

Mitochondria were attached onto a glass-based culture dishes coated with Cell-Tak® (BD Biosciences) (19). The dishes were incubated with 10 mM PQ and 2 mM NADH (Oriental Yeast Co., Ltd., Tokyo, Japan) in the sucrose solution containing 5 μM DCFH, 5 μM rotenone (Sigma-Aldrich), and 1 μM *p*-hydroxymercuribenzoate (Sigma-Aldrich) at 37 °C. Fluorescence images were captured by a digital CCD camera (Pixera Penguin 150 CL, Pixera Corp., Los Gatos, CA) attached to a microscope and were analyzed by Lumina Vision bio-imaging analysis system (Mitani Corp., Fukui, Japan). The fluorescence intensity per 1000 mitochondria was calculated, and the mean value of three areas from each sample was compared. BQ (0.3 mM), anti-VDAC1 monoclonal antibody (mAb; anti-porin 31 HL mAb, 9 μg/ml; Calbiochem), and 4,4′-diisothiocyanatostilbene-2,29-disulfic acid (DIDS; 100 μM, Sigma-Aldrich) were evaluated by addition to the reaction mixture.

Electron Microscopy

Mitochondria were transferred to a sucrose solution containing 3 mM PQ, 2 mM NADH, 5 μM rotenone, 1 μM *p*-hydroxymercuribenzoate, and the solution was reacted for 30 min at 37 °C (11, 12). Superoxide dismutase (SOD; 3000 units/ml, Sigma-Aldrich) effects were evaluated by the addition of SOD to the reaction mixture. Anti-VDAC1 mAb (3 μg/ml) effects were evaluated by preincubation with the mitochondria for 5 min at 37 °C. The reaction was stopped by the addition of cold buffer. Mitochondria were immediately centrifuged, and the packed sediments were covered with 2% glutaraldehyde in phosphate-buffered saline and fixed for 1 h. The fixed clots were prepared for electron microscopy (11) and then observed by a transmission electron microscope (JEM-1200EX, JEOL Co. Ltd, Tokyo, Japan). The percentage of intact mitochondria per area was counted, and the mean of three areas was calculated.

Growth Inhibition Assays

Growth inhibition assays were performed by the stepwise addition of PQ, according to the method described by Saotome (20). Subconfluent HeLa cells were harvested by trypsinization and were precultured on 96-well plates (3×10^3 cells per well) for 24 h. Cells were treated with 7–250 μM PQ and were then cultured for 72 h. The effects of Trolox® (a water-soluble analog of vitamin E; 1 mM, Sigma-Aldrich) were evaluated by its addition to the medium. The 50% growth inhibition toxicity (IC_{50}) was estimated at 72 h.

Extraction of NADH-PQ Oxidoreductase from the Outer Membrane

To extract NADH-PQ oxidoreductase, two-step extraction with Triton X-100, deoxycholate followed by SDS/Igepal® CA-630 was performed (21). The outer membranes were isolated from the mitochondria by discontinuous sucrose gradient centrifugation (12). The isolated outer membranes were suspended in 20 mM Tris-HCl buffer (pH 7.6) containing 1% Triton X-100, 1% sodium deoxycholate, and 1 mM EDTA. The suspensions were left to stand on ice for 1 h. Suspensions were then centrifuged at 105,000 × *g* for 60 min. The precipitates were resuspended in a 20 mM Tris buffer with 0.06% SDS and 0.1% Igepal CA-630. The suspensions were left on ice for 1 h. The supernatants were collected by centrifugation at 105,000 × *g*.

Preparation of NADH-PQ Oxidoreductase Fraction

The supernatants were diluted with 20 mM Tris-HCl buffer (pH 8.0) containing 0.03% Triton X-100 and 10% glycerol, and the dilutions were loaded onto an anion exchange column (DEAE MemSep® 1000; Millipore Corp. Billerica, MA). The columns were washed with the Tris buffer, and proteins were eluted using a NaCl gradient. The fractions containing NADH-PQ oxidoreductase were collected from 0.25–0.3 M

NaCl fractions and dialyzed against a 20 mM Tris-HCl buffer (pH 7.6) containing 0.03% Triton X-100 and 10% glycerol.

Assays of NADH-PQ Oxidoreductase Activity

NADH Oxidation—The extracts were incubated with 0.2 mM NADH in Tris-buffered saline (TBS) containing 5 μM rotenone and 1 μM *p*-hydroxymercuribenzoate at 37 °C followed by the addition of 10 mM PQ. Activities were calculated by the first-order velocity of NADH oxidation measured at $\lambda_{340\ nm}$ ($e = 6.3 \times 10^3\ M^{-1}cm^{-1}$).

O_2^- Production—O_2^- production by NADH-PQ oxidoreductase activity was assayed using a Diogenes® luminescence system (National Diagnostics Inc., Atlanta, GA). The extracts were mixed with NADH (0.1 mM), PQ (0.0012–5 mM), and Diogenes (3-fold dilution) in TBS on a 384-well plate. The effects of DIDS (100 μM) and anti-VDAC1 mAb (30 μg/ml) were evaluated by the addition of these reagents to the mixture. The total volume of the reaction mixture was 15 μl. Chemiluminescence produced by superoxide was detected by an Envision® multilabel plate reader (PerkinElmer Life Sciences).

Immunoprecipitation

The extracts were incubated with anti-VDAC1 mAb or normal mouse IgG as a control. After incubation in TBS for 90 min at 4 °C, Protein A slurries (Amersham Biosciences) were added to the solution and gently stirred for 90 min at 4 °C. The suspensions were centrifuged, and the supernatants were obtained for the assay.

Zymography and Western Blot Analysis

The NADH-PQ oxidoreductase fraction was mixed with 0.125 M Tris-HCl buffer (pH 6.8) containing 20% glycerol and 0.02% bromphenol blue (1:1, v/v), and the mixture was loaded on native-polyacrylamide gel (5–10% gradient gel; Funakoshi, Tokyo, Japan). Electrophoresis was performed at 5 mA for 5 h on ice, and the gel was immersed in 20 mM Tris-HCl buffer (pH 7.4) containing 20% glycerol, 0.25 mM nitro blue tetrazolium, 5 μM rotenone, and 1 μM *p*-hydroxymercuribenzoate. The gel was incubated with 2 mM NADH and 10 mM PQ at room temperature for 30 min and washed with TBS, and the active bands were stained by diformazan. The electrophoresed gel was blotted, and detection was performed with anti-VDAC1 mAb. Additionally, the active band was excised and subjected to SDS-PAGE followed by Western blot analysis with anti-VDAC1 mAb.

Synthesis of Biotinylated PQ

The biotinylated paraquat was synthesized in moderate yield by condensation reaction of (+)-biotin and 3-(1′-methyl-4,4′-bipyridinium)propylammonium salt, which was prepared by successive *N*-alkylation of 4,4′-bipyridine with iodomethane and 3-bromopropylamine hydrobromide. See the supplemental methods for detailed procedures.

Plasmid Construction

Human *vdac1* cDNA was isolated as an XhoI fragment by PCR and was subcloned into pUC-CAGGS expression vector (22).

Synthesis of VDAC1 Protein Using a Cell-free Protein Synthesis System

The cDNA of VDAC1 was used. For wheat cell-free protein production of VDAC proteins, the VDAC DNA templates were constructed by "split-primer" PCR (23). The first round of PCR was performed on the cDNA using 10 nM concentrations of each of the following primers: a specific primer (5′-CCACCCACCACCACCAATGGCTGTGCCACCCACGT and AODA2306 primer, 5′-AGCGTCAGACCCCGTAGAAA). Then a second round of PCR was carried out to construct the templates for protein synthesis using a portion (5 μl) of the first PCR mix: 100 nM SPu primer (5′-GCGTAGCATTTAGGTGACACT), 100 nM AODA2303 primer (5′-GTCAGACCCCGTAGAAAAGA), and 1 nM deSP6E02 (5′-GGTGACACTATAGAACTCACCTATCTCTCTACACAAAACATTTCCCTACATACAACTTTCAACTTCCTATTCCACCCACCACCACCAATG). Wheat cell-free protein synthesis of VDAC protein was carried out using a robotic synthesizer (24, 25), GenDecorder1000® (CellFree Sciences, Yokohama, Japan) as described below. First, the transcript was created from each of the DNA templates mentioned above using SP6 RNA polymerase. The synthetic mRNAs were then precipitated with ethanol and collected by centrifugation using a Hitachi R10H rotor. Each mRNA (usually 30–35 μg) was washed and transferred into a translation mixture. The translation reaction was performed in the bilayer mode (26) with slight modifications. The translation mixture that formed the bottom layer consisted of 60 A260 units of wheat germ extract (CellFree Sciences) and 2 μg of creatine kinase (Roche Diagnostics) in 25 μl of SUB-AMIX® (CellFree Sciences). The SUB-AMIX® contained (final concentrations) 30 mM Hepes/KOH at pH 8.0, 1.2 mM ATP, 0.25 mM GTP, 16 mM creatine phosphate, 4 mM dithiothreitol, 0.4 mM spermidine, 0.3 mM concentrations of each of the 20 amino acids, 2.7 mM magnesium acetate, and 100 mM potassium acetate. 125 μl of the SUB-AMIX was placed on the top of the translation mixture, forming the upper layer. After incubation at 26 °C for 17 h, the synthesized proteins were confirmed by SDS-PAGE.

Binding Assay

The synthesized VDAC1 protein was mixed with biotinylated PQ (0–1.0 μM) in TBS containing 10% EZ block (Atto Corp., Tokyo, Japan) for 1 h. The mixtures were added to Nunc Immobilizer® streptavidin plates (Nunc, Roskilde, Denmark), which were incubated for 2 h. The plates were then washed with TBS containing 0.1% Tween 20 (TTBS). VDAC1 protein bound to biotinylated PQ was detected by anti-VDAC1 mAb (Calbiochem) followed by the addition of horseradish peroxidase-conjugated second antibody. ECL plus® (GE Healthcare) was used as a substrate of horseradish peroxidase. For NADH binding assay, biotinylated NAD^+ (R&D Systems, Inc., Minneapolis, MN) was mixed with outer membrane extract, and serial dilutions of non-labeled NADH were added for 1 h. The mixtures were incubated with anti-VDAC1 mAb, which was immobilized on Nunc Immobilizer 96-well plates in 10% EZ block (Atto Corp) for 2 h. The plates were washed with TTBS to which ExtrAvidin® peroxidase (Sigma) was added followed by a wash

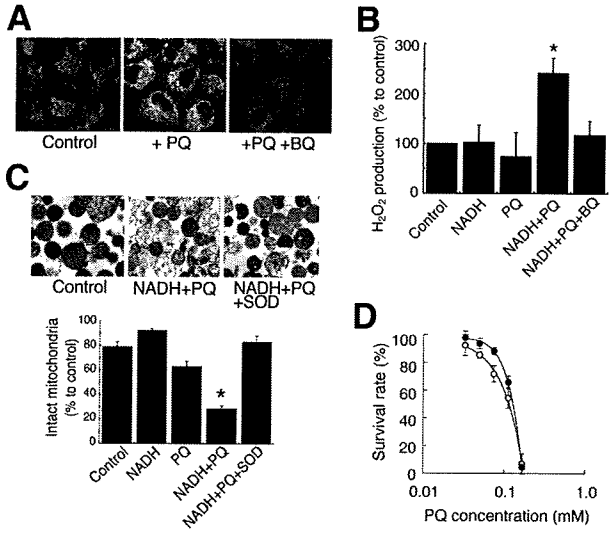

FIGURE 1. **Damage to mitochondria caused by NADH-dependent O_2^- production induced by PQ.** *A*, mitochondrial O_2^- production was visualized by MitoSOX in cells treated with PQ (1 mM) and BQ (0.2 mM). *B*, H_2O_2 production in isolated mitochondria was estimated by DCF florescence method. Mitochondria were incubated with 10 mM PQ, 2 mM NADH, and 0.3 mM BQ (*, $p <$ 0.01, *versus* control). *C*, isolated mitochondria were incubated with 3 mM PQ, 2 mM NADH, and the 3000 IU/ml SOD. *Upper panels*, electron micrograph. *Lower graph*, percentages of intact mitochondria (*, $p < 0.001$, *versus* control). *D*, the survival rate of HeLa cells exposed to PQ (*open circle*) and PQ and 1 mM Trolox® (*closed circle*). Each point is the average of two to four experiments. *Error bars* represent S.E.

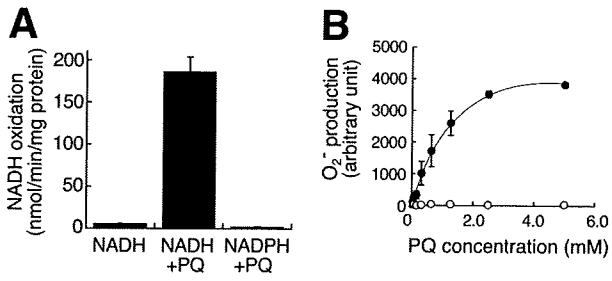

FIGURE 2. **NADH-PQ oxidoreductase activity in the outer membrane extract.** *A*, NADH (0.2 mM) was oxidized by the outer membrane extract in the presence of PQ (5 mM), but NADPH (0.2 mM) was not oxidized. *B*, PQ dose-dependent relationship to O_2^- production activity was observed by co-administration with NADH (0.1 mM) to the outer membrane extract (*closed circle*). In contrast, NADPH (0.1 mM) did not exert any such PQ effects (*open circle*). All *error bars* represent S.D. ($n = 3$).

with TTBS. ECL plus was used for the detection of binding. Immobilized normal mouse IgG was used as a control.

DNA Transfection

HeLa cells were transfected with the VDAC1 plasmid using Effectene® (Qiagen GmbH, Hilden, Germany).

Small Interfering RNA (siRNA) Transfection

HeLa cells were transfected for 72 h with 5 nM control siRNA or Hs_VDAC1_1HP_siRNA (Qiagen) using HiPerFect® transfection reagent (Qiagen).

Statistics

Statistical analyses were conducted using analysis of variance for multiple comparisons and Student's *t* test for comparing two groups.

RESULTS

PQ Produces O_2^- in an NADH-dependent Manner—We first investigated whether PQ produced ROS on mitochondria in HeLa cells. We detected O_2^- on the mitochondria using MitoSOX fluorogenic dye (Fig. 1*A*). Whereas only slight fluorescence was detected on the mitochondria in cells exposed to normal conditions, highly intense levels of fluorescence were observed when the cells were exposed to PQ. Fluorescence was reduced to the control level with the addition of BQ, a scavenger of O_2^-. In isolated rat liver mitochondria, we detected the NADH-dependent production of H_2O_2 by PQ using DCFH fluorescent dye (Fig. 1*B*). Although the fluorescence intensity did not change when PQ or NADH alone was added to the isolated mitochondria, the addition of PQ in combination with NADH raised the intensity of fluorescence in the mitochondria. BQ suppressed this augmentation. We also observed that the co-administration of PQ and NADH led to a loss of structural integrity of the isolated mitochondria, and SOD suppressed this damage (Fig. 1*C*). Furthermore, Torolox®, an O_2^- scavenger, significantly increased the survival rates of HeLa cells exposed to PQ ($p < 0.05$, Fig. 1*D*). These results indicated that PQ produced O_2^- in an NADH-dependent manner in mitochondria and damaged mitochondria followed by cell death.

VDAC1 Is Responsible for NDAH-PQ Oxidoreductase Activity—To reveal the components involved in this activity, we performed two-step extraction with Triton X-100, deoxycholate followed by SDS/Igepal CA-630 from the outer membrane and analyzed SDS/Igepal extract. The extract oxidized NADH, but not NADPH, by the addition of PQ (Fig. 2*A*), and O_2^- was produced in a PQ dose-dependent manner (Fig. 2*B*). The NADH oxidation activity was 4.4 times that of the Triton X-100/deoxycholate extract (data not shown). To ascertain whether or not VDAC protein is involved in NADH-PQ oxidoreductase activity, we examined the effects of VDAC inhibitors on this activity (Fig. 3*A*). O_2^- production by the extract from the outer membrane mixed with PQ and NADH was significantly inhibited by DIDS, an anion channel inhibitor, or anti-VDAC1 mAb, but such inhibition was not observed with exposure of the extract to normal mouse IgG. When the extract was immunoprecipitated with anti-VDAC1 mAb, the activity in the supernatant was lower than that observed with the administration of normal IgG (Fig. 3*B*). Furthermore, we confirmed that DIDS and anti-VDAC1 mAb inhibited the production of O_2^- and also inhibited the breakdown of isolated mitochondria exposed to PQ and NADH (Fig. 3, *C* and *D*). These results suggest that VDAC1 is responsible for NADH-PQ oxidoreductase activity.

VDAC1 Is Component of NADH-PQ Oxidoreductase—Because, VDAC1 protein was more highly concentrated in the SDS/Igepal extract than in the Triton X-100/deoxycholate extract (Fig. 4*A*), we investigated whether or not VDAC1 protein is contained in the oxidoreductase. We purified the active fraction from the SDS/Igepal extract using DEAE chromatography and carried out zymography on the fraction by native PAGE in blue tetrazolium solution with PQ and NADH. A

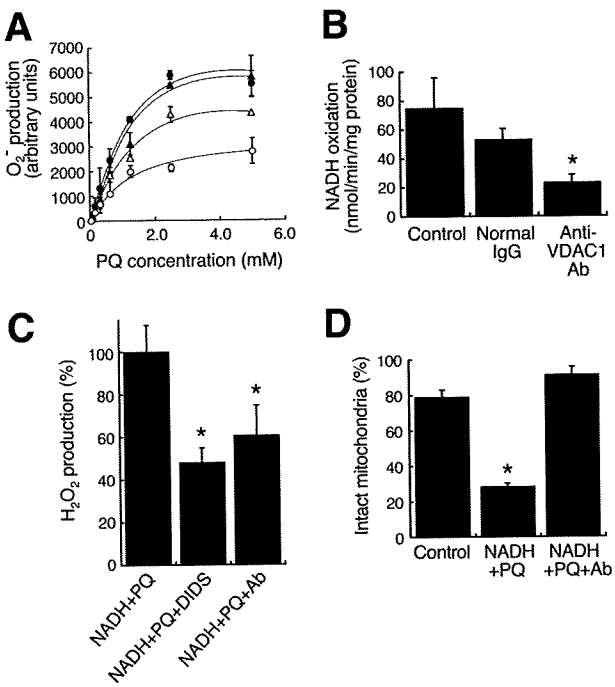

FIGURE 3. **Participation of VDAC1 in the NADH-PQ oxidoreductase activity and mitochondrial damage.** *A*, O_2^- production in the outer membrane extract (*closed circle*) was inhibited by DIDS (100 μM; *open circle*, $p < 0.001$, $n = 3$) and anti-VDAC1 mAb (30 μg/ml; *open triangle*, $p < 0.05$, $n = 3$). *Closed triangle*, treated with normal IgG (30 μg/ml). *Error bars* represent S.D. ($n = 3$). *B*, the extract was immunoprecipitated with anti-VDAC1 mAb or normal IgG, and the NADH-oxidation activity of the supernatants was measured. *Control*, no treatment. *, $p < 0.01$, *versus* control. *Error bars* represent S.D. ($n = 3$). *C*, H_2O_2 production in isolated mitochondria by PQ (10 mM) co-administered with NADH (2 mM) was estimated by DCF florescence method. DIDS (100 μM) and anti-VDAC1 mAb (9 μg/ml) were inhibited H_2O_2 production. *, $p < 0.001$ with respect to the control. Each point is the mean of triplicate experiments. *Error bars* represent S.E. *D*, effects of anti-VDAC1 antibody on the NADH-PQ-dependent breakage of mitochondria were estimated. Isolated mitochondria were ruptured by the co-administration of PQ (3 mM) and NADH (2 mM), whereas the addition of anti-VDAC1 mAb (9 μg/ml) protected the mitochondria from such breakage. *, $p < 0.01$ *versus* the control. Each point is the mean of triplicate experiments. *Error bars* represent S.E.

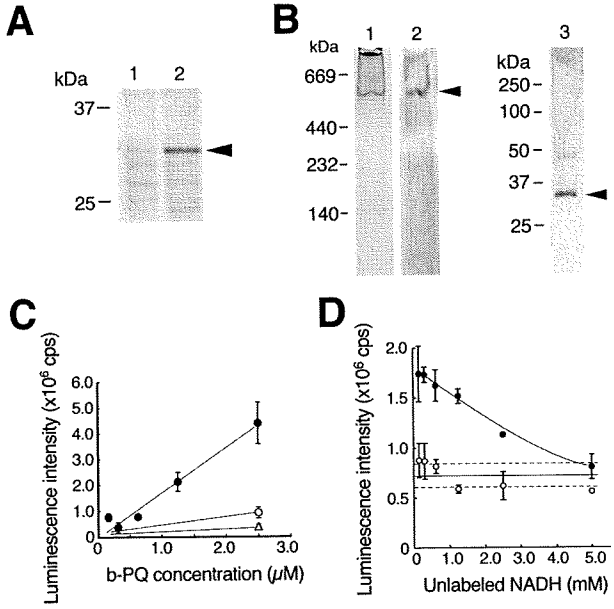

FIGURE 4. **VDAC1 is a component of NADH-PQ oxidoreductase.** *A*, extracts obtained from the mitochondrial outer membrane by treatment with Triton X-100/deoxycholate (*lane 1*) or SDS/ Igepal CA-630 (*lane 2*) were run on SDS-PAGE, and the results were analyzed by Western blotting with anti-VDAC1 mAb. VDAC1 protein was detected by the mAb (*arrowhead*). *B*, DEAE fractions from the extracts containing oxidoreductase activity were examined by zymography with NADH and PQ in blue tetrazolium solution (*lane 1*). The active band was consistent with the anti-VDAC1 mAb-detected band (*lane 2*, *arrowhead*), and this band was excised and subjected to Western blot analysis using anti-VDAC1 mAb (*lane 3*; the *arrowhead* indicates VDAC1 protein). *C*, direct binding to VDAC1 was assayed using biotinylated (*b-*) PQ (*closed circle*) in competition with non-labeled PQ (*open circle*, 25 μM, *open triangle*, 250 μM). *Error bars* represent S.D. ($n = 3$). *D*, assay of NADH binding to the outer membrane extracts was performed. The extracts were trapped by immobilized anti-VDAC1 antibody and incubated with biotinylated NAD^+. Bound biotinylated NAD^+ was reduced by exposure to non-labeled NADH ($p < 0.01$, *closed circles*). When normal IgG was used for trapping, no NADH competition was detected (*open circles*). *Broken lines* represent 95% confidence interval of the control value. *Error bars* represent S.D. ($n = 3$).

major reactive band stained with dark blue diformazan, a form of blue tetrazolium reduced by O_2^-, appeared at 500 kDa (Fig. 4*B*, *lane 1*); this band was recognized using anti-VDAC1 mAb (*lane 2*). Next, the excised band was examined by Western blot analysis with SDS-PAGE using anti-VDAC1 mAb. The antibody recognized a band at 31 kDa, the size of VDAC1 (*lane 3*). Because several proteins were detected in the reactive band by SDS-PAGE followed by silver staining (data not shown), the oxidoreductase may be a complex containing the VDAC1 protein. To confirm the direct interaction of VDAC1 with PQ, we performed a binding assay using recombinant VDAC1 protein and biotinylated PQ (Fig. 4*C*). We detected biotinylated PQ dose-dependently bound to the VDAC1 protein, and excess non-labeled PQ competed for the binding. Next, we examined the interaction of VDAC1 with NADH using biotinylated NAD^+. Whereas the biotinylated NAD^+ was not found to bind to the recombinant VDAC1 protein, which was immobilized by anti-VDAC1 mAb (data not shown), we did detect binding of the biotinylated NAD^+ using the SDS/Igepal extract instead of the VDAC1 protein (Fig. 4*D*). These results were compatible with the absence of NADH-PQ oxidoreductase activity in the recombinant VDAC1 protein or purified VDAC from rat liver mitochondria (data not shown). The present results indicate that VDAC1 is involved in NADH-PQ oxidoreductase activity as a component of the PQ binding site.

VDAC1 Is Responsible for the Cytotoxicity of PQ—Finally, we determined whether the amount of VDAC1 protein in cells affects PQ sensitivity. We obtained stable transfectants of HeLa cells overexpressing VDAC1; these cells had 2.2 times the VDAC1 protein content of control cells (Fig. 5*A*). When treated with PQ, these VDAC1-overexpressing cells showed 2.0 times the intracellular production of H_2O_2 compared with that of control cells (Fig. 5*B*). The IC_{50} of control cells exposed to PQ was 72.3 μM, and this value fell to 30.7 μM in the VDAC1-overexpressing cells (Fig. 5*C*). When HeLa cells were transfected with VDAC1 siRNA, almost no VDAC1 protein was synthesized (Fig. 6*A*). Mitochondria were isolated from these cells, and the NADH-PQ dependent H_2O_2 production was estimated (Fig. 6*B*). The production of H_2O_2 on the mitochondria from knockdown cells was reduced to endogenous levels. The sur-

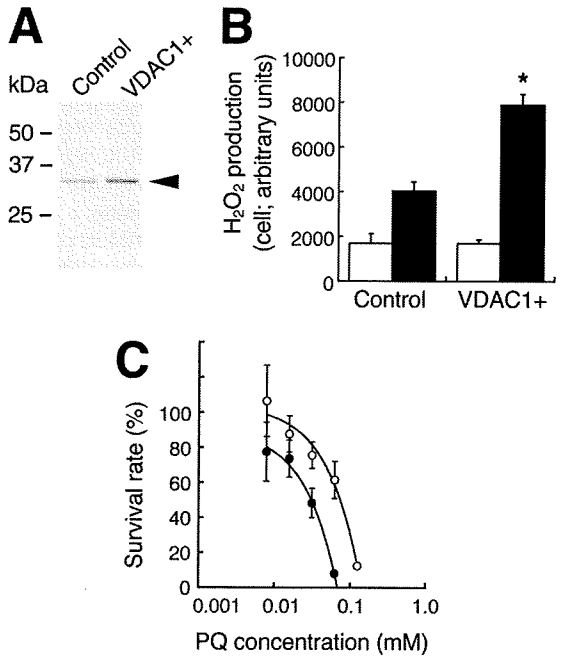

FIGURE 5. **Effects of VDAC1 overexpression on the PQ-dependent H_2O_2 production and the cytotoxicity in HeLa cells.** *A*, lysates from VDAC1-overexpressing cells were subjected to Western blot analysis with anti-VDAC1 mAb. *Control*, cells transfected with empty vector; *VDAC+*, cells transfected with the vector bearing *vdac1* cDNA. *B*, H_2O_2 production by PQ in VDAC1-overexpressing cells (*VDAC1+*) was higher than that of control cells (*, $p < 0.001$). *Light bars*, no treatment; *dark bars*, exposure to 1 mM PQ. *Error bars* represent S.D. ($n = 3$). *C*, the survival rates of VDAC1-overexpressing HeLa cells (*closed circle*) were lower than those of controls (open circle; $p < 0.001$). *Error bars* represent S.E. of triplicate experiments.

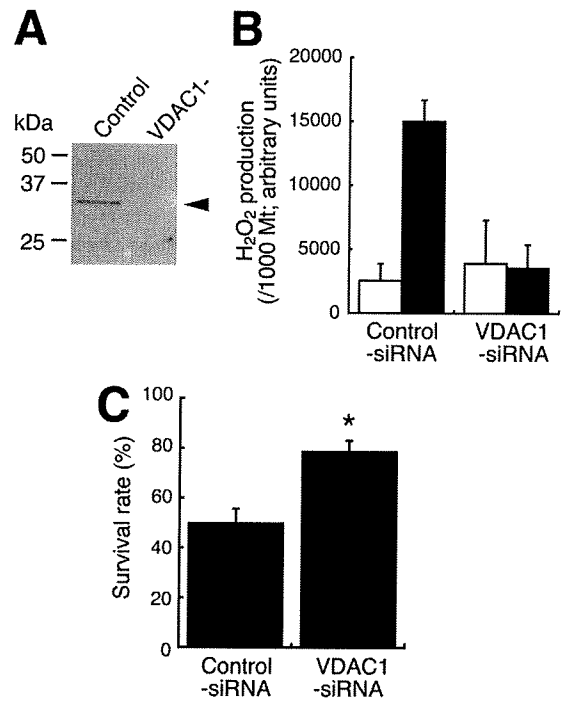

FIGURE 6. **Effects of VDAC1 knockdown on the PQ-dependent H_2O_2 production and the cytotoxicity in HeLa cells.** *A*, lysates from knockdown cells were subjected to Western blot analysis with anti-VDAC1 mAb. *Control*, cells transfected with the control siRNA; *VDAC−*, cells transfected with VDAC1 siRNA. The *arrowheads* indicate VDAC1 protein. *B*, NADH-PQ-dependent H_2O_2 production on mitochondria isolated from VDAC1-knockdown HeLa cells was estimated by DCF assay. *Light bars*, mitochondria incubated with 2 mM NADH only; *dark bars*, mitochondria were incubated with 10 mM PQ and 2 mM NADH. *Error bars* represent S.D. ($n = 3$). *C*, the survival rate of VDAC1-knockdown HeLa cells (VDA1-siRNA) after 24 h of exposure to 222 μM PQ was higher than that of control cells ($p < 0.001$). *Error bars* represent S.E. of triplicate experiments.

vival rate after exposure of the VDAC1 knockdown cells to 222 μM PQ for 24 h was 79% compared with 50% in controls (Fig. 6*C*). These results indicated that VDAC1 is responsible for the cytotoxicity of PQ as an NADH-dependent oxidoreductase.

DISCUSSION

In this study we demonstrate that a mitochondrial system, not a microsomal system, is involved in PQ poisoning; PQ produces $O_2^{\cdot-}$ by NADH-dependent oxidoreductase in the outer membrane of mitochondria and damages mitochondria, leading to cell death. Furthermore, we present that mitochondrial VDAC1 is responsible for this activity as a component of the PQ binding site.

We observed $O_2^{\cdot-}$ production on the mitochondria after administering PQ to cells using MitoSOX, an $O_2^{\cdot-}$-specific fluorescent dye. Additionally, we detected H_2O_2 production on isolated mitochondria in the presence of PQ and NADH using DCFH fluorescent dye, and BQ reduced the level of production. In a previous study we observed that cytochrome *c*, an $O_2^{\cdot-}$ scavenger, diminished H_2O_2 production on mitochondria incubated with PQ and NADH (13). Because $O_2^{\cdot-}$ is immediately (10^5 $M^{-1}s^{-1}$) converted into H_2O_2 in aqueous solution, DCF fluorescence demonstrating H_2O_2 is considered to be equivalent to a demonstration of $O_2^{\cdot-}$ production (13). We also indicated that PQ destroyed isolated mitochondria in the presence of NADH and that SOD suppressed this damage. Furthermore, Trolox® suppressed the toxicity of PQ in cells. We formerly reported that PQ selectively destroyed the mitochondria of pulmonary type II cells and hepatocyte *in vivo* (6, 11) and also destroyed cultured type II cells (7). These results indicate that PQ attacks mitochondria by NADH-dependent $O_2^{\cdot-}$ production in the course of its cytotoxicity.

In an ultrastructural study, we previously observed that NADH-dependent $O_2^{\cdot-}$ production by PQ occurred in the outer membrane of mitochondria (13) and demonstrated that the NADH oxidation activity by PQ in the outer membrane fraction was five times that of the inner membrane fraction (12). O_2 uptake on mitochondria took place with the addition of PQ and NADH (11, 12), and blue PQ radicals formed under anaerobic conditions (11). In the present study we again observed NADH oxidation and PQ radical formation in the outer membrane under anaerobic conditions (data not shown). These results indicated that an NADH-PQ oxidoreductase is localized in the outer membrane. We previously confirmed that NADH-cytochrome b_5 reductase, an outer membrane-localized oxidoreductase, did not participate in the PQ reduction, based on its insensitivity to anti-NADH-cytochrome b_5 reductase antibody and a different sensitivity to *p*-hydroxymercuribenzoate (12). We also reported that rotenone, an inhibitor of complex I in the electron

transport chain, did not inhibit NADH-dependent PQ reduction (11, 12). Intriguingly, we find that VDAC1 is a constituent of the NADH-PQ oxidoreductase. VDAC1 is a small, abundant, pore-forming protein found in the outer membranes of all eukaryotic mitochondria and plays an important role in the passage of adenine nucleotides, Ca^{2+}, and other metabolites through the outer membrane (27). In addition, VDAC1 located at contact sites between the outer and inner membranes forms permeability transition pores (PTPs) with the adenine nucleotide transporter, cyclophilin D, and other proteins (27). It is unknown whether PTP proteins besides VDAC1 participate in the NADH-PQ oxidoreductase activity; thus, it will still be necessary to investigate their involvement with PTP proteins.

Extramitochondrial oxidative stress induces PTP openings via VDAC protein without damage to the inner membrane (27). PQ does not penetrate mitochondrial membrane (28), and $O_2^{\cdot-}$ production by PQ occurs on the outer surface of the outer membrane (13). Furthermore, we demonstrated the binding of PQ to VDAC1 protein by biotinylated PQ and the inhibition of PQ-dependent mitochondrial breakage by anti-VDAC1 mAb. These results indicated that the breakage of mitochondria by PQ occurred through VDAC1. The binding mechanism of PQ, a cation molecule, to VDAC1 remains unknown. It has been reported that NADH increased the voltage dependence of VDAC and reduced the conductance of the outer membrane (29, 30). The ion selectivity of VDAC changed from anions to cations when conductance decreased (31). NADH may, therefore, affect the binding of PQ to VDAC1. Baker *et al.* (16) reported that VDAC1 localized in the plasma membrane functions as NADH-ferricyanide reductase and that VDAC1 has a putative NAD^+ binding motif. Yehezkel *et al.* (32) demonstrated that VDAC purified from rat liver mitochondria had nucleotide binding sites bound to ATP; however, NADH did not bind them. As in a previous study (Hirai *et al.* (11), the change in conformation from the orthodox to the condensed type occurred when NADH was added to starved intact mitochondria. In addition, NADH reduced the permeability of the outer membrane to ADP (15). These results indicated that NADH affects PTP even though NADH does not bind to VDAC1 directly. Although we did not observe the direct binding of NADH to VDAC1 alone, we did observe the binding of biotinylated NAD^+ to the NADH-PQ oxidoreductase concentrated extract, which was trapped by anti-VDAC1 mAb. NADH-PQ oxidoreductase activity was inhibited by DIDS and anti-VDAC1 mAb, but recombinant VDAC1 protein or purified VDAC protein alone had no activity. Therefore, an NADH binding component is expected to be necessary to yield this activity.

Yagoda *et al.* (33) reported that VDAC2 or VDAC3 was implicated in the cytotoxicity of the anti-tumor agent erastin, which was shown to induce oxidative cell death; in particular, VDAC2 was found to bind directly to this agent. We have not yet identified the involvement of VDAC2 or VDAC3 in NADH-PQ oxidoreductase activity. It has been reported that VDAC1 is the most abundantly expressed of the three VDAC isoforms in mammalian mitochondria (34). In addition, we demonstrated a correlation between the production of $O_2^{\cdot-}$ and VDAC1 expression, and we observed defective $O_2^{\cdot-}$ production on the mitochondria isolated from VDAC1 knockdown cells. Therefore, it appears that VDAC1 participates primarily in NADH-PQ oxidoreductase activity. Recently, we found that several furanonaphthoquinones caused mitochondrial damage and the apoptosis of cancer cells by the production of ROS, and other studies revealed that VDAC1 induces ROS production by an NADH-dependent quinone reduction (17, 35). Additionally, we previously demonstrated that menadione, a naphthoquinone, was a substrate of NADH-PQ oxidoreductase (12). These previous and present results taken together suggest that the function of VDAC1 is not only to serve as a channel but also to function as part of an oxidoreductase enzyme.

Until now, management of PQ poisoning has been directed primarily at removing PQ from the gastrointestinal tract by the use of several absorbents (activated charcoal, Fuller's Earth, etc.) and increasing its excretion from the blood by hemoperfusion (2). However, the efficacy of these treatments is poor. Our results indicated that $O_2^{\cdot-}$ production by a VDAC-containing mitochondrial system is responsible for PQ poisoning. DIDS and anti-VDAC1 antibody inhibited NADH-PQ oxidoreductase activity, mitochondrial $O_2^{\cdot-}$ production, and the breakage of mitochondria by PQ. Furthermore, PQ cytotoxicity was suppressed in VDAC1-knockdown cells. These results suggest that specific VDAC inhibitors can be therapeutic agents of PQ poisoning.

Acknowledgment—We are grateful to Mayumi Mitani for secretarial assistance.

REFERENCES

1. Wesseling, C., van Wendel de Joode, B., Ruepert, C., León, C., Monge, P., Hermosillo, H., and Partanen, T. J. (2001) *Int. J. Occup. Environ. Health* **7,** 275–286
2. Dinis-Oliveira, R. J., Duarte, J. A., Sánchez-Navarro, A., Remião, F., Bastos, M. L., and Carvalho, F. (2008) *Crit. Rev. Toxicol.* **38,** 13–71
3. McCormack, A. L., Thiruchelvam, M., Manning-Bog, A. B., Thiffault, C., Langston, J. W., Cory-Slechta, D. A., and Di Monte, D. A. (2002) *Neurobiol. Dis.* **10,** 119–127
4. Baldwin, R. C., Pasi, A., MacGregor, J. T., and Hine, C. H. (1975) *Toxicol. Appl. Pharmacol.* **32,** 298–304
5. Bus, J. S., Cagen, S. Z., Olgaard, M., and Gibson, J. E. (1976) *Toxicol. Appl. Pharmacol.* **35,** 501–513
6. Hirai, K., Witschi, H., and Côté, M. G. (1985) *Exp. Mol. Pathol.* **43,** 242–252
7. Wang, G. Y., Hirai, K., and Shimada, H. (1992) *J. Electron Microsc. (Tokyo)* **41,** 181–184
8. Yang, W., and Tiffany-Castiglioni, E. (2005) *J. Toxicol. Environ. Health A* **68,** 1939–1961
9. St. Clair, D. K., Oberley, T. D., and Ho, Y. S. (1991) *FEBS Lett.* **293,** 199–203
10. Oliver, P. D., and Newsome, D. A. (1992) *Invest. Ophthalmol. Vis. Sci.* **33,** 1909–1918
11. Hirai, K., Ikeda, K., and Wang, G. Y. (1992) *Toxicology* **72,** 1–16
12. Shimada, H., Hirai, K., Simamura, E., and Pan, J. (1998) *Arch Biochem. Biophys* **351,** 75–81
13. Hirai, K. I., Pan, J., Shimada, H., Izuhara, T., Kurihara, T., and Moriguchi, K. (1999) *J. Electron Microsc. (Tokyo)* **48,** 289–296
14. Shimada, H., Furuno, H., Hirai, K., Koyama, J., Ariyama, J., and Simamura, E. (2002) *Arch. Biochem. Biophys.* **402,** 149–157
15. Lee, A. C., Xu, X., and Colombini, M. (1996) *J. Biol. Chem.* **271,** 26724–26731
16. Baker, M. A., Lane, D. J., Ly, J. D., De Pinto, V., and Lawen, A. (2004) *J. Biol. Chem.* **279,** 4811–4819

17. Simamura, E., Hirai, K., Shimada, H., Koyama, J., Niwa, Y., and Shimizu, S. (2006) *Cancer Biol. Ther.* **5,** 1523–1529
18. Ariyama, J., Shimada, H., Aono, M., Tsuchida, H., and Hirai, K. I. (2000) *Intensive Care Med.* **26,** 981–987
19. Nakayama, S., Sakuyama, T., Mitaku, S., and Ohta, Y. (2002) *Biochem. Biophys. Res. Commun.* **290,** 23–28
20. Saotome, K., Morita, H., and Umeda, M. (1989) *Toxicol. In Vitro* **3,** 317–321
21. Teraoka, K., and Matsui, S. (1999) *Nippon Rinsho.* **57,** (suppl.) 784–788
22. Narita, M., Shimizu, S., Ito, T., Chittenden, T., Lutz, R. J., Matsuda, H., and Tsujimoto, Y. (1998) *Proc. Natl. Acad. Sci. U.S.A.* **95,** 14681–14686
23. Sawasaki, T., Ogasawara, T., Morishita, R., and Endo, Y. (2002) *Proc. Natl. Acad. Sci. U.S.A.* **99,** 14652–14657
24. Sawasaki, T., Kamura, N., Matsunaga, S., Saeki, M., Tsuchimochi, M., Morishita, R., and Endo, Y. (2008) *FEBS Lett.* **582,** 221–228
25. Sawasaki, T., Gouda, M. D., Kawasaki, T., Tsuboi, T., Tozawa, Y., Takai, K., and Endo, Y. (2005) *Methods Mol. Biol.* **310,** 131–144
26. Sawasaki, T., Hasegawa, Y., Tsuchimochi, M., Kamura, N., Ogasawara, T., Kuroita, T., and Endo, Y. (2002) *FEBS Lett.* **514,** 102–105
27. Crompton, M. (1999) *Biochem. J.* **341,** 233–249
28. Gage, J. C. (1968) *Biochem. J.* **109,** 757–761
29. Lee, A. C., Zizi, M., and Colombini, M. (1994) *J. Biol. Chem.* **269,** 30974–30980
30. Zizi, M., Byrd, C., Boxus, R., and Colombini, M. (1998) *Biophys. J.* **75,** 704–713
31. Vyssokikh, M., and Brdiczka, D. (2004) *Mol. Cell. Biochem.* **256–257,** 117–126
32. Yehezkel, G., Hadad, N., Zaid, H., Sivan, S., and Shoshan-Barmatz, V. (2006) *J. Biol. Chem.* **281,** 5938–5946
33. Yagoda, N., von Rechenberg, M., Zaganjor, E., Bauer, A. J., Yang, W. S., Fridman, D. J., Wolpaw, A. J., Smukste, I., Peltier, J. M., Boniface, J. J., Smith, R., Lessnick, S. L., Sahasrabudhe, S., and Stockwell, B. R. (2007) *Nature* **447,** 864–868
34. Yamamoto, T., Yamada, A., Watanabe, M., Yoshimura, Y., Yamazaki, N., Yoshimura, Y., Yamauchi, T., Kataoka, M., Nagata, T., Terada, H., and Shinohara, Y. (2006) *J. Proteome Res.* **5,** 3336–3344
35. Simamura, E., Shimada, H., Ishigaki, Y., Hatta, T., Higashi, N., and Hirai, K. I. (2008) *Anat. Sci. Int.* **83,** 261–266

Tsukasa Seya
Misako Matsumoto
Takashi Ebihara
Hiroyuki Oshiumi

Functional evolution of the TICAM-1 pathway for extrinsic RNA sensing

Authors' address
Tsukasa Seya[1], Misako Matsumoto[1], Takashi Ebihara[1], Hiroyuki Oshiumi[1]
[1]Department of Microbiology and Immunology, Hokkaido University Graduate School of Medicine, Sapporo, Japan.

Correspondence to:
Tsukasa Seya
Department of Microbiology and Immunology
Hokkaido University Graduate School of Medicine
Kita 15, Nishi 7, Kita-ku
Sapporo 060-8638
Japan
Tel.: +81 11 706 5073
Fax: +81 11 706 7866
e-mail: seya-tu@pop.med.hokudai.ac.jp

Acknowledgements
We thank Drs A. Matsuo, T. Tsujita, A. Ishii, M. Shingai, M. Sasai, and K. Funami in our laboratory for their valuable discussions. This work was supported in part by CREST, JST (Japan Science and Technology Corporation), and by Grants-in-Aid from the Ministry of Education, Science, and Culture (Specified Project for Advanced Research) and the Ministry of Health, Labor, and Welfare of Japan, and by the Takeda Science Foundation, Uehara memorial Foundation, Northtec Foundation, Akiyama Foundation and Mitsubishi Foundation. Financial supports by the Sapporo Biocluster 'Bio-S' the Knowledge Cluster Initiative of the MEXT, and the Program of Founding Research Centers for Emerging and Reemerging Infectious Diseases, MEXT are gratefully acknowledged.

Immunological Reviews 2009
Vol. 227: 44–53

Immunological Reviews
0105-2896

Summary: The type I interferon (IFN) is a host defense factor against microbial pathogens in vertebrates. In mammals, retinoic acid-inducible gene I (RIG-I) and melanoma differentiation-associated gene 5 (MDA5) in the cytoplasm are regarded as sensors for double-stranded RNA (dsRNA) and trigger IFN regulatory factor-3 (IRF-3) activation followed by type I IFN induction through the mitochondrial antiviral signaling (MAVS) adapter. This intrinsic pathway appears to link the main protective responses against RNA virus infection in mammals. On the other hand, human Toll-like receptor 3 (TLR3) is localized in the endosomal membrane or cell surface and signals the presence of extrinsic dsRNA. In response to RNA stimulation, TLR3 recruits the Toll-interleukin 1 receptor domain (TIR)-containing adapter molecule 1 (TICAM-1) adapter and induces IRF-3 activation followed by IFN-β promoter activation. Human TLR3 is localized limitedly extent in myeloid dendritic cells, fibroblasts, and epithelial cells. The TICAM-1 and cytoplasmic MAVS pathways converge at the IRF-3-activating kinase in human cells. The reason for the involvement of this extrinsic mode of IFN-inducing pathways in the dsRNA response remains unknown. In fish, two TLRs, i.e. endoplasmic TLR3 and cell surface TLR22, participate in teleost IFN production without the activation of IRF-3. TLR22 is distinct from mammalian TLR3 in terms of cellular localization, ligand selection, and tissue distribution. TLR22 may be a functional substitute for human cell surface TLR3 and may serve as a surveillance molecule for detecting dsRNA virus infection and alerting the immune system for antiviral protection in fish. In this review, we discuss the fundamentals of the extrinsic dsRNA recognition system, which has evolved to induce cellular effectors to cope with dsRNA virus infection across different vertebrate species.

Keywords: *Toll-like receptor, evolution, dsRNA recognition, TICAM-1 (TRIF)*

Introduction

Invading pathogens express specific pattern molecules and are recognized by host pattern recognition receptors (PRRs) (1, 2), representatives of which are Toll-like receptors (TLRs), Nod-like receptors (NLRs), and RNA helicases [retinoic acid-inducible gene I (RIG-I), melanoma differentiation-associated protein 5 (MDA5), etc.]. These receptors signal the presence of microbial patterns in myeloid dendritic cells (mDCs) and thus induce potent activation of the systemic host defense response (3). Recent studies on pattern receptors of

the innate immune system have increased our understanding of how mDCs mature through infection and subsequently orchestrate cellular immunity (4, 5). These molecules also serve as adjuvants for the induction of antigen-specific acquired immunity. TLRs, RIG-I-like helicases (RLHs), and NLRs are major targets for investigating the induction of robust acquired immune responses upon pathogen stimulation. These studies have been conducted using gene-disrupted mice and in *in vitro* human systems.

It has been reported that human cells induce interferon-β (IFN-β) in response to various RNA structures (6, 7). Double-stranded RNA (dsRNA) and its analog polyinosinic–polycytidylic acid (polyI:C) have been identified as potent immune stimulators of viral patterns and are recognized by PRRs. PRRs link cytoplasmic adapter molecules in these mammalian cells. Cytoplasmic RLH and membrane-associated TLRs that induce IFN-α/β involve the mitochondrial antiviral signaling (MAVS) (also known as IPS-1, Cardif, or VISA) or TICAM-1 [Toll-interleukin-1 receptor (IL-1R) (TIR) domain-containing adapter-inducing IFN-β (TRIF)] adapters, respectively, to converge the signal at IRF-3-activating kinases for IFN-β induction (4, 5, 8). IFN-β induction is IRF-3 dependent in mDCs and fibroblasts/epithelial cells (4, 5). By contrast, IFN-α/β is differentially induced in an IRF-7-dependent manner in plasmacytoid DCs (pDCs) (9). This allows activation of the myeloid differentiation factor 88 (MyD88) adapter protein and IKKα [inhibitor of nuclear factor (NF) κB (IκB) kinase α] kinase, which directly activates the IRF-7 transcription factor (10). However, the molecular assembly and mechanism involved in polyI:C-mediated activation of transcription factors still remain unclear in mice and humans.

Some PRRs preferentially recognize nucleic acid structures that are unique to infectious microbes. Type I IFN induction and cytotoxic T-lymphocyte (CTL)/natural killer (NK) cell activation are major outputs for RNA-sensing PRRs in mammalian cells (5, 11). A variety of RNA sensors in the cytoplasm or membranes are engaged in the detection of microbial RNA. These are expressed in a cell-type specific fashion and participate in IFN-α/β production in various cell types. However, the combinations of these receptors that induce cellular immunity still remain undetermined. It is generally accepted that RNA patterns that are exogenously provided or are produced in bystander cells are internalized by mDCs through phagocytosis and are then recognized by endosomal PRRs. By contrast, RNA patterns produced in the cytoplasm of infected cells are directly recognized by PRRs present in the cytoplasm (12). In this review, we adopted an evolutional approach to study TLRs present on the cell membrane and the recognition of the external dsRNA pattern that is specifically formed in other cells during virus replication.

Fish (teleost) have >20 TLRs that include orthologs of human TLRs and other TLRs unique to lower vertebrates living in water (13, 14). Teleost have orthologs of the IFN-inducing genes of mammals and PRRs for microbial pattern recognition. Teleost also have a TICAM-1 ortholog which has no TRAF-binding site but retains the RIP1-binding site (15, 16). Fish may have orthologs of RLH and NLRs. Hence, by comparing the mammalian PRR receptor/adapter system with that of fish, it is possible to examine the development of the innate recognition system during evolution. Molecular evolution by which the mammalian immune system has been established in the current form can be analyzed through the genomic information of vertebrate TLR systems. In this study, we cast insight into the functional properties of fish TLRs and adapters involved in IFN induction.

Recognition of RNA duplexes in vertebrates

Viral replication usually generates dsRNA in the cytoplasm of infected cells and signals to activate antiviral responses. dsRNA, stem-loop structure of RNA, 5′-uncapped triphosphate of RNA, and specific RNA sequences are rapidly recognized by PRRs in the cytoplasm (4, 5, 17), then implicated in host defense (*Fig.* 1). Many pattern-sensing receptors have been identified in mammals: PKR (dsRNA-dependent protein kinase), Dicer of the short interfering/microRNA system, RLHs including RIG-I, MDA5, and LGP2, and other helicases. These receptors are accompanied by adapters that transduce the dsRNA-sensing signal downstream. Other RNA-sensing molecules such as helicases may also be present in the cytoplasm to join a molecular assembly for foreign RNA detection. The synthesized dsRNAs are incorporated into these molecular complexes to prohibit RNA replication in virus-infected cells.

TLR3 is present in the early endosome and can recognize dsRNA delivered inside the endosomal membrane (18). TLR3 may not have a direct role in capturing dsRNA generated by virus replication in the cytoplasm, but it has an important role in trapping phagocytosed dsRNA (*Fig.* 2), which is usually wrapped in a membrane that originates from the infected cell (19). In comparison to the direct recognition system of dsRNA in the cytoplasm, this mode of RNA recognition is unique and sophisticated, concerning activation of cellular immunity. As RNA-sensing TLRs and RLH are conserved across vertebrates (20), we hypothesize

